Annals of Biomedical Engineering, Vol. 24, pp. 1–24, 1996
Printed in the USA.

0090-6964/96 $10.50 + .00

Simulation of Intraluminal Gas Transport Processes in the Microcirculation

J. DAVID HELLUMS,* PRETEP K. NAIR,† NANCY S. HUANG,‡ and NORIO OHSHIMA§

*Cox Laboratory for Biomedical Engineering, Rice University, Houston, TX; †Chemshare, Inc., Houston, TX; ‡Exxon Production Research Corp., Houston, TX; and §Department of Biomedical Engineering, Institute of Basic Medical Sciences, The University of Tsukuba, Tsukuba, Ibaraki, Japan

Abstract—Intraluminal resistance to gas transport between the microcirculation and tissue was neglected for a half-century following the early work of Krogh. In recent years it has come to be understood that this neglect is seriously in error. This paper reviews the background for the long period of misdirection, and progress in placing the simulation of gas transport processes on a more accurate, quantitative basis.

Keywords—Oxygen transport, Oxygen, carbon dioxide transport, Mathematical models, Microcirculation, Blood, Erythrocytes, Capillaries, Arterioles, Hemoglobin.

INTRODUCTION

The literature on mathematical analysis of mass transfer-related processes in the microcirculation has grown greatly in recent years. A relatively complete simulation of O_2 and CO_2 transport would encompass a very complicated series of chemical reaction and transport processes taking place in numerous media arranged in geometrically complex and heterogeneous ways. Therefore, of necessity, all treatments invoke numerous simplifying assumptions to reduce the very complex situation to one that is mathematically tractable. One of the pervasive problems in this sphere of activity is the difficulty of obtaining experimental data of sufficient detail and accuracy to permit critical testing and validation (or invalidation) of the different sets of simplifying assumptions used by the various workers. Nevertheless, significant progress has been made on a number of fronts, and one of the purposes of this review is to outline some of this progress for a small subset of the general simulation problem.

In this review, attention is directed entirely to intraluminal processes—and to those associated with oxygen release and carbon dioxide uptake within the vessels of the microcirculation. Understanding of and ability to predict the intraluminal resistance to transport can be regarded as building blocks needed to simulate the transport to tissue in any configuration. The intraluminal resistance was entirely neglected in Krogh's classic work (55,56), and this approach was followed by almost all investigators for the next half-century. In recent years, our understanding of the distribution of resistances has changed dramatically, and now it is clear that the intraluminal resistance is of at least equal importance as that in the surrounding tissue. Therefore, it is appropriate that the progress in this restricted intraluminal focus be reviewed. The reader is referred to other reviews (67,69) for overviews of several other aspects of oxygen transport.

This review has three principal parts: a brief review of fundamentals and of recent important progress in mathematical simulation methods; results of calculations on oxygen release in arteriolar-size and larger vessels and in capillary-size vessels; and a review of a recent study on simulation of simultaneous oxygen and carbon dioxide transport. The results of calculations on oxygen release are presented in terms of mass transfer coefficients, which can be used to predict oxygen transport rates. The mass transfer coefficients can readily be incorporated into the (necessarily much more complicated) models for simulation of the microcirculatory networks in tissue. It will be shown that the resistance to oxygen transport in the arteriolar-size vessels is substantial and must be taken into account in an accurate simulation. Almost without exception previous workers have neglected this important resistance. In addition, the important interactions between oxygen and carbon dioxide transport have been neglected in many previous studies.

REVIEW OF PREVIOUS THEORETICAL WORK ON OXYGEN RELEASE IN THE MICROCIRCULATION

Oxygen Transport in Hemoglobin Solutions

Equilibrium and Kinetic Expressions. The great majority of the oxygen in oxygen-saturated hemoglobin solutions is

Acknowledgment—This work was supported by a grant from the Special Research Project of the Circulation Biosystem at The Institute of Basic Medical Sciences of the University of Tsukuba.

Address correspondence to Professor J. David Hellums, Cox Laboratory for Biomedical Engineering, Rice University, 6100 South Main Street, Houston, TX 77005, U.S.A.

(Received 29Aug95, Revised 21Sep95, Revised, Accepted 21Sep95)

carried in chemically bound form. The oxyhemoglobin dissociation process often is represented by the simple one-step reversible reaction

$$HbO_2 \leftrightarrow Hb + O_2 \quad (1)$$

Here Hb represents one of the four heme group in each hemoglobin molecule, and the net rate of liberation of oxygen from oxyhemoglobin, R_{O_2}, per unit volume could be given by

$$R_{O_2} = k[HbO_2] - k'[Hb][O_2] \quad (2)$$

where brackets denote concentration, and k and k' are the dissociation and association reaction velocity coefficients, respectively. These reaction velocity coefficients sometimes are assumed to be constants. A correspondingly simplified equation for the rate of oxygen release in which these coefficients are not necessarily constants will be discussed below. At equilibrium, the net rate of reaction, R_{O_2}, is zero. Because of the large size of the hemoglobin molecule, it is safe to assume that the diffusion coefficients of Hb and HbO_2 are essentially identical. With this knowledge, it is easy to show that the total hemoglobin concentration remains constant. $[Hb_T]$ denotes the total (oxy plus deoxy) heme concentration (the heme concentration is four times the hemoglobin concentration because there are four heme groups on each hemoglobin molecule). Substitution of $[Hb] = [Hb_T] - [HbO_2]$ and rearrangement of Eq. 2 with $R_{O_2} = 0$, yields an expression for equilibrium in terms of S, the hemoglobin oxygen saturation, defined to be $[HbO_2]/[Hb_T]$:

$$S = \frac{(k'/k)[O_2]}{1 + (k'/k)[O_2]} \quad (3)$$

If k and k' are treated as constants, Eq. 3 constitutes a hyperbolic curve that deviates sharply from the measured equilibrium curve (Fig. 1). The problem was recognized early and treated by Adair (1), who noted that each molecule of oxygen added to the hemoglobin molecule yields a chemically different species with a different binding affinity and different reaction velocity coefficients. Accordingly, in the Adair model, Eq. 1 is replaced with a set of four equations, and there are eight reaction velocity coefficients. When the Adair model is reduced to the equilibrium condition, it represents the measured equilibrium curve well.

To avoid using the mathematically complex Adair model, Moll (61) proposed that Eqs. 1 and 2 be used, but that one of the two coefficients be varied to ensure compatibility with the experimentally determined equilibrium curve.

Many curve fits have been made to the observed equilibrium curve (see, for example, 66). The oldest and most widely known curve fit is the Hill (41) equation (Fig. 1), which gives a satisfactory fit over the range of saturations of most physiological interest.

It is common practice to express the dissolved oxygen concentration in terms of oxygen tension (oxygen tension is a synonym for oxygen partial pressure). The relationship between oxygen tension, P_{O_2}, and dissolved oxygen concentration, $[O_2]$, is through the Bunsen solubility coefficient, α,

$$[O_2] = \alpha P_{O_2} \quad (4)$$

where typical values of α are 1.50×10^{-6} M/torr in red blood cells, α_{rbc} (36), and 1.34×10^{-6} M/torr in plasma, α_{pl} (69), and M is molar concentration g moles/l.

In terms of P_{O_2} and S, the Hill equation can be written as follows:

$$S = \frac{(P_{O_2}/P_{50})^n}{1 + (P_{O_2}/P_{50})^n} \quad (5)$$

or in inverse form as

$$P_{O_2}/P_{50} = \left(\frac{S}{1 - S}\right)^{1/n} \quad (6)$$

where P_{50} is the oxygen tension that yields $S = 0.50$, and n is an empirical constant.

The Moll approach replaced the constant dissociation coefficient k of Eqs. 2 and 3 with the variable k given by Eq. 7.

$$k = \alpha k' P_{50} \left[\frac{S}{1 - S}\right]^{\frac{1}{n} - 1} \quad (7)$$

This substitution assures compatibility with the Hill equation. In other words, setting $R_{O_2} = 0$ in Eq. 2 gives the Hill equation when Moll's choices of k and k' are used.

Instead of the Moll approach of using the constant association coefficient k', Clark *et al.* (14) used a constant dissociation coefficient, $k = 44\ s^{-1}$, and varied the association constant to obtain compatibility with the equilibrium curve. The approach of Clark *et al.* (14) has been adopted by others (*e.g.*, 63,87). It seems to have an advantage over the Moll approach in that it is better behaved at low oxygen tensions.

Some workers have noted that the Hill equation is not very accurate at high ($S > 0.90$) and low ($S < 0.10$) saturations and, as a result, use fixed values of k and k' in the end regions (57,86,87).

The importance of using a kinetic expression compatible with the observed equilibrium curve is illustrated in Fig. 1. Calculations that use a simple model that invokes fluxes of the order of those in the microcirculation were conducted using constant values of k and k' (5). This choice makes the kinetic expression compatible with the

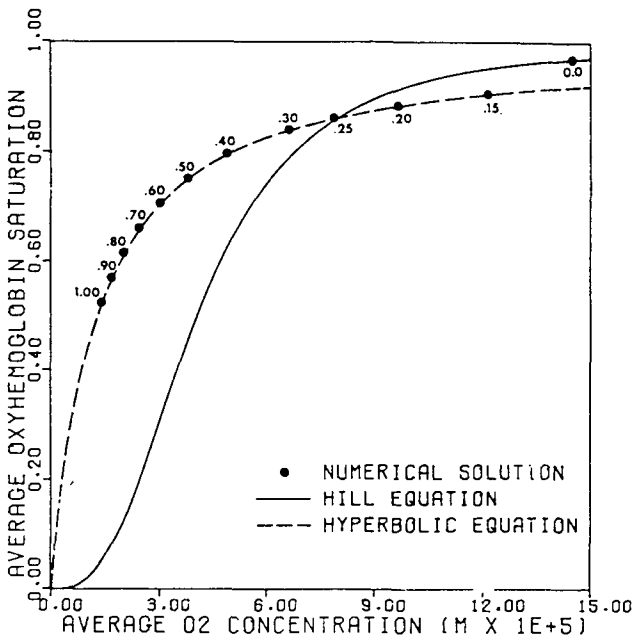

FIGURE 1. Comparison of the oxygen-oxyhemoglobin equilibrium curves by the hyperbolic equation, Eq. 3 and the Hill equation, Eq. 5. The numbers along the curve denote residence time in seconds for an erythrocyte as it traverses the capillary. The concentrations are calculated by use of a simple model for oxygen delivery to tissue involving mass action kinetics of the single-step type, Eq. 2, with constant reaction velocity coefficients. (Adapted from Reference 5.)

hyperbolic equilibrium curve, Eq. 3, as shown in Fig. 1. The points shown were averaged through the hemoglobin layer as calculated for various times of retention of an erythrocyte as it traverses the microcirculation (times are indicated along the curve). It can be seen that, after a short initial transient period, the calculated points fall very close to the hyperbolic equilibrium curve and, hence, are erroneous. In contrast, when the calculations were repeated with the Moll approach, the calculated points (data not shown) were almost indistinguishable from the Hill equation, which is a more accurate depiction of the observed equilibrium curve. These and other results show that the local oxygen and hemoglobin concentrations are in a condition of near equilibrium in the microcirculation. Therefore, having accurate values of the reaction velocity coefficients k and k' is much less important than having their ratio ensure compatibility with the equilibrium curve. This point was demonstrated by Yap and Hellums (94). In this work, calculations of fluxes under conditions typical of the microcirculation were made using the Adair four-step model in comparison with the Moll model. In a comparison of this type, one must keep in mind the question being asked. If the Adair model describes a different equilibrium curve than the Moll model, we know *a priori* that the oxygen concentrations and fluxes calculated will be different. Therefore, the question is the following: Does a reaction kinetic model on a sound basis (Adair) have important practical advantages over a model (Moll) in which a reaction velocity coefficient is varied with no experimental basis or constraint other than compatibility with equilibrium? To address this question, the calculations were made with coefficients that describe the same equilibrium curve. The resultant oxygen tension distributions and oxygen fluxes were almost indistinguishable, thereby confirming that use of the Adair model is not essential. The much simpler variable-coefficient models are entirely adequate in practical calculations of oxygen fluxes in the physiologic range.

Facilitation of Oxygen Transport by Diffusion of Oxyhemoglobin. The facilitation of oxygen transport by diffusion of oxyhemoglobin is known to be an important mechanism for oxygen transport under some circumstances. The basic idea of this facilitation is illustrated in Fig. 2, in which we imagine a layer of hemoglobin solution between two membranes that are permeable to oxygen but not to hemoglobin (as in a red blood cell). One side has a high oxygen tension, and the other side has a low oxygen tension. As a result, we have a diffusive flux of oxygen down the concentration gradient. Superimposed on the diffusion of dissolved oxygen, we have oxygen carried in a chemically bound form by the hemoglobin. The increase in oxygen transport caused by the diffusion of oxyhemoglobin is designated facilitation. On the high oxygen tension side, hemoglobin tends to load with oxygen and then diffuse down the concentration gradient to the lower oxygen tension side, where the hemoglobin unloads oxygen and diffuses back in the deoxygenated state. Keller and Friedlander (51) showed experimentally that, in dilute hemoglobin solutions, the facilitation can increase O_2 transport as much as eightfold over ordinary O_2 diffusion. Sheth and Hellums (80) performed calculations that showed that, under conditions typical of the normal microcirculation (concentrated hemoglobin solutions), facilitation may increase transport by as much as a factor of two.

The enhancement, E, is defined as the actual oxygen flux divided by what the flux would be if there were no facilitation (if there were only diffusion of dissolved oxygen). The enhancement of oxygen transport can be calculated easily for a simple case such as that illustrated in Fig. 2 (51,56) as follows:

$$E = 1 + \frac{D_{HbO_2}}{D_{O_2}} M \tag{8}$$

where D_{HbO2} is the diffusivity of oxyhemoglobin, D_{O2} is the diffusivity of dissolved oxygen, and M is the slope of the oxyhemoglobin-oxygen equilibrium curve given by Eq. 9:

$$M = \frac{\partial[HbO_2]}{\partial[O_2]} \tag{9}$$

In a more general approach the total oxygen flux can be determined by use of an effective diffusivity, D_{eff} defined by

$$j_{O_2} = -D_{eff}\nabla[O_2] \quad (10)[1]$$

where j_{O_2} is the total flux of oxygen by diffusion, and $\nabla[O_2]$ is the gradient of the oxygen concentration. Because the total flux is a result of diffusion of both oxygen and oxyhemoglobin, we have

$$j_{O_2} = -D_{O_2}\nabla[O_2] - D_{HbO_2}\nabla[HbO_2] \quad (11)$$

and for equilibrium,

$$\nabla[HbO_2] = \frac{\partial[HbO_2]}{\partial[O_2]}\nabla[O_2] = M\nabla[O_2] \quad (12)$$

we have

$$D_{eff} = D_{O_2} + MD_{HbO_2} \quad (13)$$

It should be noted that these expressions assume that the oxygen and oxyhemoglobin are in local chemical equilibrium. In view of the earlier statements about the near-equilibrium condition, it appears that the assumption of chemical equilibrium would be adequate in mathematical models of oxygen transport in hemoglobin solutions. As will be discussed below, it is somewhat paradoxical that often it is not so. One cannot invoke the simplifying assumption of chemical equilibrium without neglecting the phenomenon of facilitated diffusion. Therefore, one must use caution in using the simple expression of effective diffusivity.

The Problem with the Equilibrium Assumption. The difficulty with the equilibrium assumption is easily visualized for a simple case such as that illustrated in Fig. 2. The equilibrium assumption means that the values of $[O_2]$ and $[HbO_2]$ are directly related through the equilibrium curve. At the boundaries of the layer of Fig. 2, we see that there is no hemoglobin flux. Therefore, by Fick's law, we have a zero normal gradient of $[HbO_2]$ at the boundary, as shown in Eq. 14:

$$\frac{\partial[HbO_2]}{\partial n} = 0 \quad (14)$$

However, through the equilibrium relationship, Eq. 14 implies that the oxygen concentration normal gradient at the boundary also is zero. Therefore, we have the unacceptable imposition of a zero oxygen flux through the boundary.

The conclusion is that, although the oxygen and hemoglobin are in a condition of near equilibrium throughout most of the layer illustrated in Fig. 2, there must always be a thin region near the boundary, the boundary layer, in which the deviation from chemical equilibrium is significant. As a result, many workers in mathematical simulation use the more complete set of differential equations, such as Eqs. 15 and 16 (below), which contain the chemical reaction rate expressions. These equations are highly nonlinear and usually require numerical solution.

A different approach was used by Clark *et al.* (14). They assumed chemical equilibrium except in the boundary layer and used the method of matched asymptotic expansions to treat the deviation from chemical equilibrium in the boundary layer. Through this analysis, they obtained an analytical solution for the rate of deoxygenation of erythrocytes.

Equations for Oxygen Transport in Hemoglobin Solutions. Under the assumption of uniform total hemoglobin concentration, we require balance equations for only two species, oxygen and oxyhemoglobin, as follows:

$$\frac{\partial[O_2]}{\partial t} + \bar{v}\cdot\nabla[O_2] = D_{O_2}\nabla^2[O_2] - R_{O_2} \quad (15)$$

and

$$\frac{\partial[HbO_2]}{\partial t} + \bar{v}\cdot\nabla[HbO_2] = D_{HbO_2}\nabla^2[HbO_2] - R_{O_2} \quad (16)$$

where $\bar{v}$ denotes the fluid velocity vector.

These equations are simplified for various situations; for example, Lemon *et al.* (57) treated the case of steady-state flow and oxygen transport in a cylindrical conduit. They neglected diffusion in the axial (z), or flow,

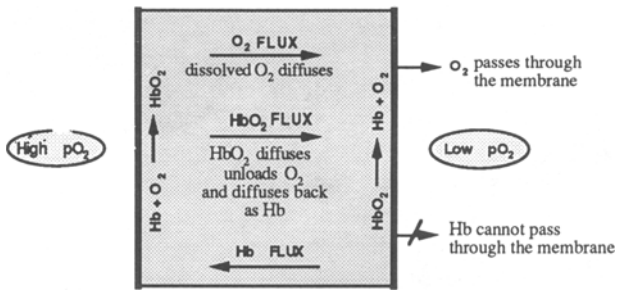

FIGURE 2. Schematic representation of the mechanism for facilitated diffusion of oxygen in hemoglobin solutions.

[1]Throughout this paper and the literature on oxygen transport, a simplified form of Fick's law, which tacitly—and correctly—assumes low concentrations of the diffusing species, is used. Therefore, Fick's law has been written as if it were for a binary system with constant total concentration.

direction and assumed no flow in the radial direction. These simplifications yield Eqs. 17 and 18:

$$v\frac{\partial[O_2]}{\partial z} = D_{O_2}\left\{\frac{\partial^2[O_2]}{\partial r^2} + \frac{1}{r}\frac{\partial[O_2]}{\partial r}\right\} - k'[Hb][O_2] + k[HbO_2] \quad (17)$$

$$v\frac{\partial[HbO_2]}{\partial z} = D_{HbO_2}\left\{\frac{\partial^2[HbO_2]}{\partial r^2} + \frac{1}{r}\frac{\partial[HbO_2]}{\partial r}\right\} + k'[Hb][O_2] - k[HbO_2] \quad (18)$$

where v is the axial fluid velocity, z is the axial space coordinate (distance from the capillary entrance), and r is the radial space coordinate. They used the parabolic expression for the velocity distribution characteristic of laminar flow of a Newtonian flow (7):

$$v = \frac{2Q}{\pi r_c^2}[1 - (r/r_c)^2] \quad (19)$$

where Q is the volumetric flow rate, and r_c is the radius of the conduit.

The equations were solved by Lemon *et al.* (57) to simulate oxygen uptake and release experiments in the artificial capillary system of Boland *et al.* (8–10). The very good agreement between calculated and experimentally determined oxygen transport parameters was regarded as a validation of the relatively difficult experimental measurements, because the theory of diffusion and reaction in homogeneous hemoglobin solutions is on a firm theoretical basis.

Simulations in Which Intraluminal Resistance to Oxygen Transport is Neglected

Krogh's early work (54,55) has served as a basis for much of the subsequent work. His approach included use of a typical capillary, assumed to be cylindrical, surrounded by a annular ring of tissue, the Krogh tissue cylinder, which exchanges mass with and only with the one typical capillary. The radius of the tissue cylinder was assumed to be one half the estimated typical capillary spacing in the tissue. This approach yielded the important mathematical simplification of axial symmetry. Therefore, only two space dimensions are considered. In most analyses, axial diffusion in both the tissue and the blood is neglected, but axial convection in the blood is taken into account. The rate of oxygen consumption or disappearance per unit of volume of tissue often is assumed to be a constant, although more complicated expressions sometimes are used in conditions of anoxia. In most studies, steady state is assumed. A key point is that the diffusion problem within the capillary was ignored by Krogh and by most subsequent workers for many years under the tacit assumption that the resistance to mass transfer within the tissue was dominant.

In other studies, the tissue that contains capillaries, but not larger blood vessels, was treated as a continuum (71,74,75,92). In other words, the oxygen tension distribution was regarded as smoothed by a volume-averaging procedure, and the scale of the averaging procedure was assumed to be large relative to the capillary spacing. Under these assumptions, the mean oxygen concentration can be represented as a single concentration that can be determined by solving a single partial differential equation. The objective of this approach is to gain information on the overall oxygen concentration distribution pertinent to the whole organ level, without treating the small scale variations. This approach (92) and an earlier approach used by Popel and Gross (70) have been applied to describe the oxygen tension distribution and oxygen fluxes in the vicinity of precapillary, arteriolar blood vessels. In these approaches, the radial oxygen tension gradient in the arterioles was neglected similar to the way in which the Krogh approach neglected the capillaries. The results of this work presumably give insight into the gradients and fluxes for such cases, but it is outside the scope of this paper's focus on intraluminal processes. In addition, it would appear that the accuracy of these methods could be improved by the incorporation of the radial oxygen tension gradient within the arterioles. Below, in "Comparison of Calculated Results with *In Vivo* Results," we show that such gradients constitute a significant fraction of the overall gradient in the tissue and, therefore, are far from negligible.

Early Treatment of the Intraluminal Resistance to Oxygen Transport

Following Krogh's approach, the intraluminal resistance to oxygen transport was entirely neglected for about forty years. In 1960, Thews (85) observed that the Kroghian flat oxygen tension profile in the capillary was not possible, since diffusion of oxygen requires a partial pressure gradient, and since the oxygen is released by a reversible chemical reaction with hemoglobin. Thews treated the diffusion-reaction problem in a simplified, linear form and gave an estimate of the intraluminal oxygen tension gradient.

Subsequently, Reneau *et al.* (72,73) gave the first detailed treatment of the intraluminal oxygen transport processes. They treated the blood as a continuum—as if it were a homogeneous hemoglobin solution—and assumed local chemical equilibrium. They incorporated convection in the axial or flow direction, and radial diffusion. They solved the convection-diffusion problem in the capillary and the diffusion problem in the tissue simultaneously and matched the two solutions as they evolved by using the

appropriate boundary conditions of continuity in both oxygen tension and oxygen flux. They treated a number of transient and steady-state problems and investigated the importance of axial diffusion in both the blood and in the tissue (it was found to be of negligible importance in the blood and of significant but slight importance in the tissue). Because this model is highly nonlinear, Reneau *et al.* (72,73) and most subsequent workers have used numerical methods to solve the system of partial differential equations.

The equations used by these workers can be obtained from Eqs. 17 and 18 by using the following procedure: 1) neglect the term involving D_{HbO_2} in Eq. 16 (the facilitation effect); 2) add Eqs. 17 and 18, thereby eliminating R_{O_2}, which is positive in one equation and negative in the other; and 3) note that under the equilibrium assumption, derivatives of $[HbO_2]$ can be expressed in terms of derivatives of $[O_2]$, as given earlier by Eq. 12.

The effect of the velocity profile was investigated by solving for cases of plug flow (v constant) and for cases of parabolic flow (Eq. 19). Extensive calculations were made over a wide range of values of the parameters. Representative results are given in Figs. 3 and 4, which show the effects of reduced hematocrit on oxygen tension profiles and on anoxic regions of tissue.

This early work should be regarded as a turning point in simulation of oxygen transport to tissue. The work stimulated a number of other workers to study intraluminal processes and to extend and improve the models. In addition, several workers used the calculated results of Reneau *et al.* (72,73) as the basis or test case to evaluate simpler models (48,58,83). Lightfoot (58) showed that, for the steady-state case, the oxygen tension profile approached its asymptotic shape within a few microns of the capillary entrance, and that it was possible to get a simple analytical solution which gave a good approximation to the numerical solutions.

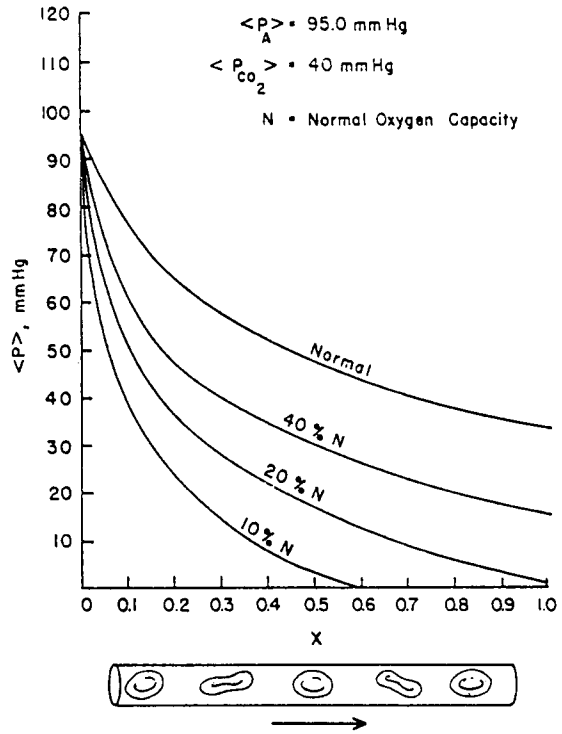

FIGURE 3. Calculated axial oxygen partial pressure profiles in the capillary showing the effect of reduced erythrocyte concentration in blood entering a capillary. All other conditions are normal. Numbers along the *abscissa* are fractions of the total capillary length. (From Reference 73, with permission.)

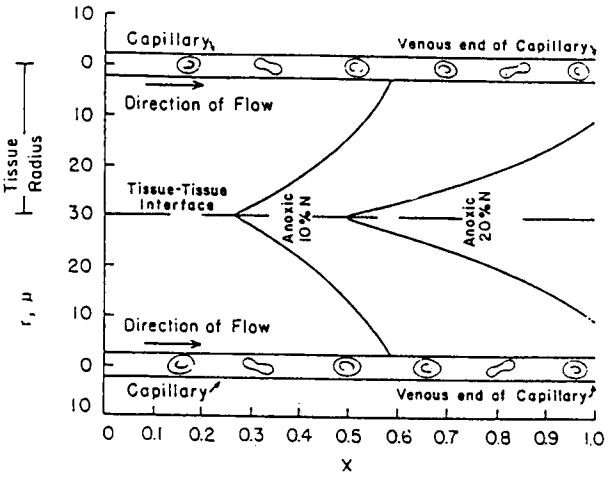

FIGURE 4. Calculated anoxic areas (volumes) of tissue between parallel capillaries with concurrent flow resulting from reduced erythrocyte concentration. All other conditions are normal. Tissue radius is measured in microns. (From Reference 52, with permission.)

Continuum Versus Discrete Cell Models

As indicated above, most early workers neglected completely the resistance to oxygen transfer in the blood. Those few workers who did consider the blood diffusional resistance treated blood as a continuum. This treatment of blood as a continuum was examined in 1977 (39) by use of a simple model suggested by the geometrical configuration of erythrocytes in capillaries. The sketch given in Fig. 5 was based on the cell lengths and clearances measured by Hochmuth *et al.* (42) and by Seshadri *et al.* (79). In a 4-μm-diameter capillary, the red blood cells (RBCs) deform to an almost cylindrical shape, which nearly fills the lumen of the capillary, and the space between the cells is approximately equal to the deformed cell length (for a 45% hematocrit) (42,82). Several workers (2,12,22) have shown that radial convection currents are of only secondary importance. Therefore, it seems clear that, in the small capillaries, the transport of oxygen primarily is radial through the erythrocyte and through the narrow plasma gap between it and the capillary wall. Furthermore, bearing in mind the fact that nearly all of the oxygen

is transported in the erythrocytes, it is clear that the effective capillary surface area for oxygen transfer to the tissue is only approximately 50% of the total capillary area—and less for lower hematocrits.

A second source of error in the earlier work on the continuum approach lies in the diffusivity along the diffusion path. As seen in Fig. 5, for small capillaries, diffusion occurs for the most part in the concentrated hemoglobin solution in the erythrocyte. The effective diffusivity in the concentrated solution is only approximately 50% of that used in the continuum approach (based on the overall average hemoglobin concentration).

There are erythrocyte-associated transients in the oxygen tension and oxygen flux—from the standpoint of an observer fixed in space on the capillary wall. (These transients are discussed below.) An order of magnitude argument was used to indicate that these transients were of only secondary importance, and the problem was treated as a steady-state case in which, for a 45% hematocrit, the oxygen flux at the erythrocyte boundary was twice that at the capillary wall (taken to be uniform). This concept of the fluxes is illustrated in Fig. 9, adopted from the work of Groebe (36).

These factors were taken into account in a simple extension of Lightfoot's solution and matched with a Krogh-type diffusion solution for the tissue. The result was an analytical expression for the relative resistance to oxygen transport in the capillary and the tissue. Values of the relative resistance compared with that in the corresponding continuum case were found to be insensitive to the values of the single parameter, the ratio of the Krogh tissue cylinder radius to the capillary radius. The fractional resistance in the capillary was found to be approximately 50% in the discrete cell approach and approximately 20% in the continuum approach. This finding is in contrast with the assumption of most early workers who followed Krogh and neglected the resistance in the blood entirely. Even the few early workers who did consider the resistance underestimated its importance.

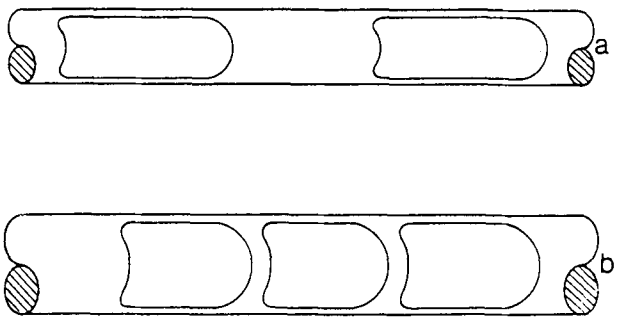

FIGURE 5. Sketch illustrating the important influence of capillary diameter on the geometrical parameters associated with the oxygen transfer process: (a) 4-μm capillary; (b) 6-μm capillary. In both cases, the geometrical parameters correspond to a 45% hematocrit (Reproduced with permission from [40]).

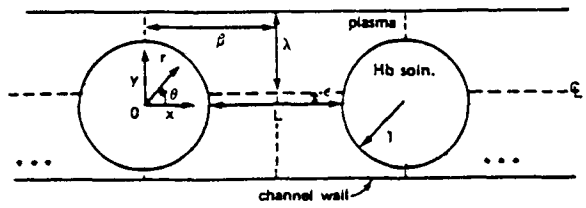

FIGURE 6. Schematic of model geometry. Geometry is either two-dimensional or axisymmetric three-dimensional; in the latter case, particle eccentricity, ϵ, is zero. (From Reference 27, with permission.)

Improved Discrete Cell Models

The analysis outlined above had a number of simplifications and limitations that required examination.

Baxley and Hellums (5) extended the analysis to include facilitated transport and chemical reaction kinetics by using the same simple geometry, and obtained results consistent with the main finding: approximately 50% of the resistance to oxygen delivery is within the capillary. They also obtained the findings on the variable rate kinetic expression and of the importance of compatibility with equilibrium discussed earlier.

Federspiel and Sarelius (28) and Federspiel and Popel (27) advanced the discrete cell model by exploring the influence of the key parameter of erythrocyte spacing (related to hematocrit), as well as the influence of a number of other parameters, and by taking diffusion in the plasma gaps between cells into account. Their most interesting calculations (27) used the idealized geometric configuration of spherical RBCs suspended in a cylindrical conduit as shown in Fig. 6.

The authors expressed their results in terms of a dimensionless mass transfer coefficient, k^*, which is a mass transfer Nusselt number, Nu (a notation used by some other workers and to be used in this paper later)

$$k^* = \frac{j_w r_c}{(P^* - P_w D_{pl}\alpha_{rbc}} \tag{20}$$

where j_w is the mass flux of oxygen from the capillary to the tissue,[2] D_{pl} is the diffusivity of oxygen in the plasma, P^* is the oxygen tension in equilibrium with the mixed mean[3] hemoglobin saturation in the RBC, and P_w is the oxygen tension at the capillary wall.

Results expressed in terms of k^* were found to be almost independent of both oxygen saturation in the RBCs and the flow velocity, but they were found to depend

[2]Mass flux is used as the rate per unit area for mass transfer per unit time (*e.g.*, g mol/(cm^2-sec). Several workers in the microcirculation use flux to be per unit length of capillary instead of per unit area. Still others use the term flux to denote total mass transfer rate (*e.g.*, g mol/sec).

[3]Mixed mean values are defined in "A Model for the Pre- and Post-Capillary Microcirculation," following.

strongly on RBC spacing in the capillary as shown in Fig. 7. Also shown in Fig. 7 is the significant but weaker effect of cell clearance, expressed as $\lambda = r_c/a$, where a is particle radius. In Fig. 7, L is the edge-to-edge space between particles expressed as multiples of particle length, $2a$. This work forms a very useful basis from which to examine the prime determinants of the resistance to oxygen release from RBCs, although, as we noted, it is not expected that the values calculated would describe precisely the oxygen release *in vivo*—in large part because of the simplified geometry used. The key finding was the extreme importance of the cell spacing parameter.

Groebe and Thews (38) extended the treatment of the effects of cell spacing in a study on oxygen delivery to canine skeletal muscle. The RBC geometry was approximated by solid cylindrical slugs analogous to the schemes of Figs. 5, 8, and 9. They noted that the previous work by Federspiel and Popel (27), Federspiel and Sarelius (28), and Homer *et al.* (43) had, in a sense, treated the RBCs as motionless. Therefore, there was neglect of the interaction between moving RBCs and the stationary tissue. This interaction may be characterized as "charging" and "discharging" of the stationary structure with oxygen as an RBC or a plasma gap, respectively, passes by. The results obtained by Groebe and Thews (38) show that the RBC motion tends to equalize the variations in boundary P_{O_2} and O_2 flux of the static models. There were significant calculated variations in flux or P_{O_2}, but these variations were shown to dampen rapidly with depth in the surrounding tissue. The net effect of the RBC motion on the average oxygen delivery to the muscle tissue of their model was an increase of approximately 10%. It was concluded that nonuniformity of O_2 flux out of capillaries as a result large RBC gaps did not play an important role for tissue O_2 supply as long as average RBC spacing was sufficiently small to guarantee an appropriate overall capillary flux. Some results of this study by Groebe and Thews (38) are presented below.

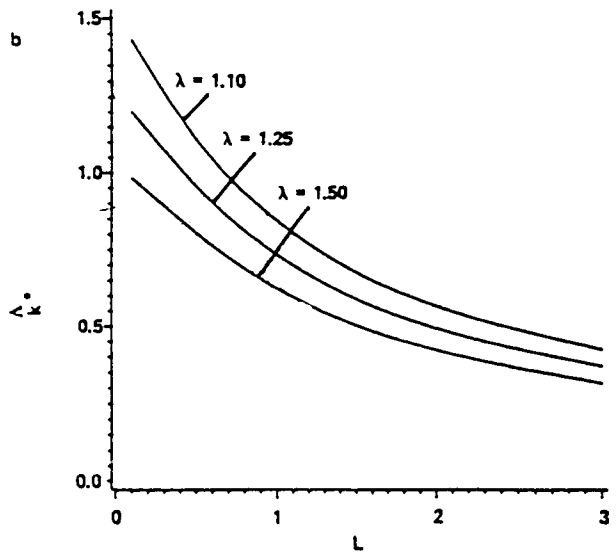

FIGURE 7. Effect of particle spacing, L, and particle clearance, λ, on the capillary mass transfer coefficient for the axisymmetric three-dimensional case. Shown is the average capillary mass transfer coefficient from $\hat{S}$ = 80% to $\hat{S}$ = 20%, k^*, as discussed in the text. L is in units of particle lengths. (From Reference 27, with permission. Legend was modified slightly.)

In related work, Secomb *et al.* (78) studied the effects of sinusoidal oscillations in tissue P_{O_2} imposed at the capillary wall. The amplitude of the fluctuation decayed with depth in the tissue in a frequency-dependent manner. Relatively low frequency fluctuations (0.2 Hz), characteristic of vasomotion, persist throughout radial distances in the tissue typical of capillary spacing. Higher frequency fluctuations (20 Hz), characteristic of the erythrocyte-induced transients discussed in above, penetrate only a few μ into the tissue and do not reach the regions in which anoxia is most likely to occur. Therefore, their conclusions were consistent with those of Groebe and Thews (38).

Groebe and Thews (35–39) have undertaken a number of other studies in which they simulated the oxygen supply to muscle. The focus of much of their work is on the oxygen tension and myoglobin saturation distributions in and around the muscle fibers. However, they have used complete models, including intraluminal capillary resistance. One difference between their approach and those of other workers is that they do not treat the intraluminal resistance as a separate entity. Instead, they consider three regions, usually annular in shape, as illustrated in Fig. 8. In order of increasing radius they treat: 1) the RBC, approximated as cylinders; 2) an annular carrier-free region (CFR) surrounding the RBCs; and 3) the muscle tissue. The carrier-free region is lumped together in the calculations, but it is thought of as representing three entities: 1) the plasma layers between the RBCs and the capillary wall; 2) the endothelial cells of the capillary wall; and 3) the interstitial space outside and immediately adjacent to the capillary. Typical dimensions in the work of Groebe and Thews are of a 4-μm-diameter red cell in the capillary surrounded by a 1.55-μm-thick annular ring of CFR. The CFR typically is taken to contain a 0.75-μm layer of plasma (giving a 5.5-μm diameter capillary) plus a 0.8-μm layer of endothelium and interstitial space. The muscle tissue containing the carrier myoglobin, surrounds the CFR. In contrast, other workers typically treated the capillaries as 3.6–5 μm in diameter, in which the RBCs are surrounded by an annular plasma layer of 0.2–1.0 μm thickness and the endothelium and interstitial space are treated as part of the surrounding tissue. Groebe and Thews (38) have treated the intra-RBC part of the oxygen transport problem by solving Eqs. 15 and 16, or, in some cases, by using the solution of Clark *et al.* (14).

Groebe (35,36) has evaluated the procedure used by

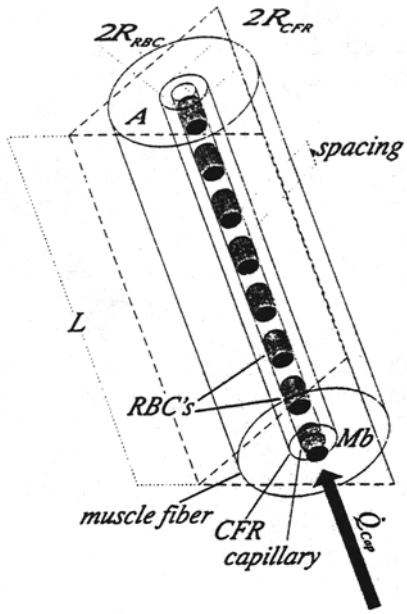

FIGURE 8. Schematic drawing of capillary domain geometry in muscle. A capillary domain (large circular or triangular cylinder) of length *L* and cross-sectional area *A* is supplied out of a central capillary, which is perfused by a given blood flow Q_{Cap}. Adjacent RBCs (radius R_{RBC}) within the capillary are separated by plasma-filled gaps (spacing). Most of the capillary domain is occupied by the muscle fibers in which myoglobin (Mb) serves as a oxygen carrier. Erythrocytes and muscle fiber are separated by a carrier-free region (CFR, radius R_{CFR}), which is made up of a perierythrocytic plasma sleeve, the capillary endothelium, and interstitial space. (From Reference 36, with permission.)

Baxley and Hellums (5) and by Hellums (39) in which the radial oxygen flux is assumed to be non-zero in the capillary only at locations adjacent to the RBCs and is assumed to be uniform in the surrounding tissue at the capillary-tissue interface. This approach is illustrated in Fig. 9. It can be regarded as the limiting case in which the charging and discharging phenomena discussed above are entirely smoothed out because of the high frequency of the passing RBCs. The approach was found to give results that were almost identical to those given by more detailed calculations over a range of conditions. Of course, the idealization should be questioned in severe anemia, in which large intererythrocyte gaps occur.

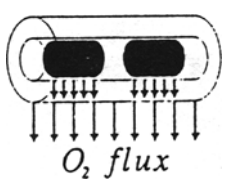

FIGURE 9. The present model assumes radial O_2 flux in the CFR adjacent to RBCs only, and uniform radial O_2 flux in the muscle fiber. (From Reference 36, with permission. The legend is from the original figure and, therefore, refers to that work.)

A sample of the results obtained by Groebe and Thews (38) is given in Fig. 10, in which we see the oxygen tension distribution in a muscle fiber and three surrounding capillaries. The dramatically large drop in oxygen tension seen in and in the near vicinity of the capillaries was in marked contrast to the relatively small gradients in the muscle fiber tissue. These distributions have been shown to be in good qualitative agreement with the experimental measurements of Gayeski and Honig (33,34) and are in remarkable disagreement with the Krogh approach.

The Need for Different Models for Different Vessel Diameters

There are at least five regimes in which very different approaches were needed to model oxygen transport processes in blood. Three of these regimes are of most direct interest *in vivo* and are discussed first.

1.) For true capillaries in the diameter range of 4 or 5 μm, the solid cylinder shape approximation seems to be sound. The major dimension of a human RBC

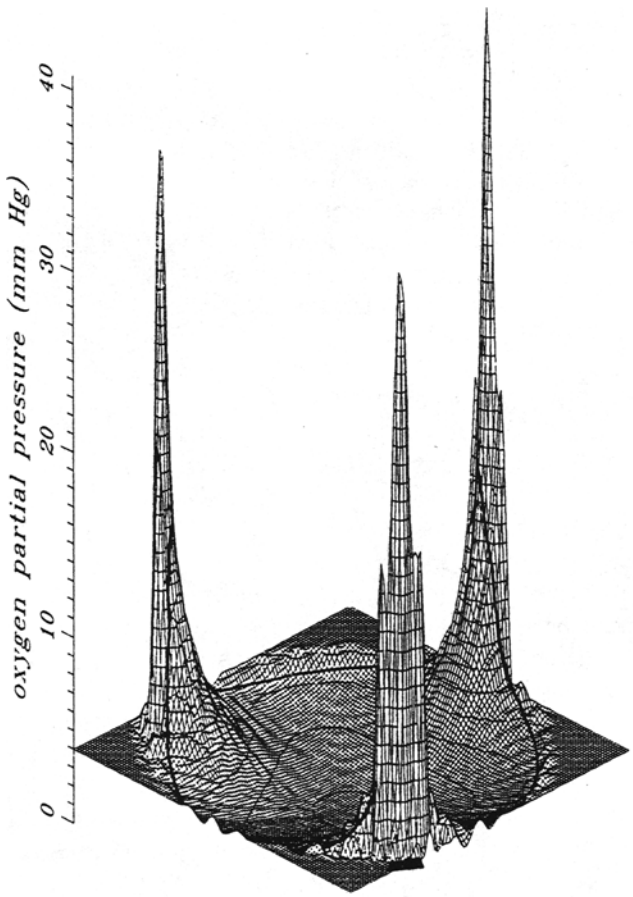

FIGURE 10. P_{O_2} distribution inside muscle fiber and carrier-free layer, which are surrounded by three blood-perfused capillaries. The bold line outlines the boundary of the muscle fiber. The position of a RBC in the capillary next to the observer is symbolized by a black area. (From Reference 97, with permission.)

is approximately 8 μm. It is known that, in the capillaries, the RBCs deform about an axis parallel to the cylinder axis into a shape that has been described as resembling a "slipper" with a length approximately that of the RBC major dimension, 8 μm (32). A question in the cylinder approach might be how to deal with the asymmetrical aspect of the deformed cell, the "inside" of the slipper. As shown previously (43), from examination of the micrographs of Gaehtgens *et al.* (32), there cannot be much space unoccupied by the RBC inside the "slipper" in small capillaries. Consider a solid cylinder of 2 μm in radius and 8 μm in length, which is typical of the cylinder model. Such a cylinder's volume is 100 $(\mu m)^3$, which is in approximate agreement with the actual RBC volume. Therefore, the solid cylinder idealization for small capillaries seems to have a good geometrical basis, and it has the important property of simplicity. Results from this approach are given in "Numerical Values of the Mass Transfer Coefficients for Oxygen Delivery to the Wall of Microvessels."

2.) For arteriolar-sized and larger microvessels, 20–100 μm in diameter, Nair *et al.* (62–64) have developed a model that treats the particulate nature of blood in a pseudo-continuum way that takes into account the nonuniform hematocrit distribution in the vessel. This model has been validated by comparison with experiment and is discussed below.

3.) For vessels of intermediate size, 8–15 μm, little work has been done. In these vessels the assumption of a continuous hematocrit distribution used by Nair *et al.* is almost certainly inadequate, and the cell motion is much more complicated than is the single file motion of the small capillaries. One study in this regime was performed by Wang and Popel (91) based on the cell shapes calculated for an 8.24-μm-diameter vessel by Zarda *et al.* (95). Zarda *et al.* (95) used a model that assumed a single file flow, in which the starting, undeformed shape of the RBC was oriented with its major axis normal to the axis of the capillary. Then, the RBC deformed in an axially symmetric, "parachute" shape under the influence of the stresses associated with flow. Wang and Popel (91) found that this shape change significantly altered oxygen delivery—this in itself is an interesting finding. However, there is no experimental evidence for the specific cell orientation and shapes used by Zarda *et al.* (95). Therefore, although the results are of interest in indicating the effects of shape change, they cannot be expected to give highly accurate predictions of *in vivo* oxygen delivery.

Two other regimes, which are not directly used in *in vivo* simulations and, thus, are outside the scope of this paper, are described below in brief.

4.) For relatively large vessels, 200 μm and larger, several workers have observed that RBCs rotate and make excursions from the streamlines of the time-averaged flow. This RBC motion enhances solute transport. This enhancement has been taken into account in a continuum approach to simulations by use of effective diffusivities that depend on shear rate (11,16–21,25,88–90,96).

5.) Many basic studies of RBC reactions, especially reaction kinetics, have used the "stopped-flow" reactor. In these experiments, for example, oxygenated RBC can be mixed directly and immediately with a deoxygenated fluid or a fluid containing an oxygen scavenger (86,87). In this way, extremely high RBC oxygen fluxes can be obtained, and studies can be made of both reaction kinetics and transport processes. Therefore, useful basic information is obtained, although the RBC oxygen fluxes are outside the physiologic range.

A Model for the Precapillary and Postcapillary Microcirculation

It has been observed that a significant fraction of the microcirculatory oxygen transport occurs in arterioles and venules (23,24,71). Thus, it is important that we be able to predict oxygen transport processes in larger vessels (20 μm diameter and larger), as well as in capillaries. This section focuses on the transport in these larger vessels, where the hydrodynamics and mass transfer characteristics are known to differ from those of the capillaries.

Boland *et al.* (8–10) have developed an experimental *in vitro* system to study oxygen transport processes in small cylindrical conduits. In this *in vitro* system, the intracapillary and extracapillary resistances to oxygen transport can be determined separately and accurately. This section, from the work of Nair *et al.* (62–64), concerns the development of a mathematical model for arteriolar-sized vessels and the use of results from the experimental system of Boland *et al.* (8–10) and from other previous studies to validate the model for microcirculatory oxygen supply or uptake.

Physical Problem and Outline of Approach. The flow of RBCs through large microvessels is more complex that is the single file flow in the small capillaries of the microcirculation. The RBCs more or less retain their disc shape in the large microvessels. The overall flow profile has been observed to be parabolic with a light blunting at the center. Because of the shear field, the RBCs tend to move away from the wall, resulting in a relatively cell-free layer close to the wall. This movement leads to a radial distribution of hematocrit with a higher hematocrit at the center and lower hematocrit near the walls.

Because the RBCs are semisolid entities suspended in the plasma, the velocities of the cells and the plasma as well as various properties such as hematocrit vary with position in a discontinuous way. However, as a simplification these quantities are treated as varying continuously.

Therefore, for example, the RBC velocity at a given radial position is an average over time, even though at any given instant of time the particular position may or may not be occupied by an RBC.

Hematocrit and Velocity Profiles. From observations of hematocrit profiles it has been found that the radial hematocrit distribution can be expressed as

$$h(r) = h_m[1 - (r/r_r)^m] \quad 0 \leq r \leq r_r$$
$$h(r) = 0 \quad r_r \leq r \leq r_c \qquad (21)$$

where r is the radial coordinate, $h(r)$ is the hematocrit, the volume fraction RBCs at any radius r; r_r is the radius of the cell-rich region; and h_m and m are constants. The distribution is of the form suggested by Lih (59), with a modification to exclude the cell-free region.

Different velocity profiles were used for the plasma and the RBCs (Fig. 11). The profiles are parabolic with a slight blunting and differ by a constant—the slip, *slp*

$$v'_{pl} = A[1 - (r/r_c)^2] \quad r_r \leq r \leq r_c \qquad (22a)$$

$$v_{pl} = G[1 - B(r/r_c)^2] \quad 0 \leq r \leq r_r \qquad (22b)$$

$$v_{rbc} = G(1 - slp)[1 - B(r/r_c)^2] \quad 0 \leq r \leq r_c \qquad (22c)$$

where B is the blunting factor [taken to be 0.9, based on the work of Pittman and Ellsworth (68)], representing deviation from the Poiseuille flow parabolic profile, $v'_{pl}(r)$ is the plasma velocity at radius r in the cell-free region, $v_{pl}(r)$ is the plasma velocity at radius r in the cell-rich region, *slp* is a slip constant taken to be 0.10 based on work by Sinha (81), and v_{rbc} (r) is the *rbc* velocity at radius r in the cell-rich region.

The velocity variables have the property that $hv_{rbc}(r)$ gives the local volumetric flux of RBCs (volume of RBCs per unit time per unit area). Similarly $(1 - h)v_{pl}(r)$ is the local volumetric flux of plasma. A sketch of the profiles is given in Fig. 11.

Oxygen Transport Relationships and a Simpler Model. The system of equations used in the more complete of the two models discussed is described below.

The dissolved oxygen balance within the RBCs takes into account convection in the axial direction, chemical kinetics of release or uptake of oxygen from oxyhemoglobin, and the local flux of oxygen between the RBC and plasma phases. The oxyhemoglobin balance within the RBCs also takes into account both convection and chemical kinetics but, of course, with no flux between phases. The oxygen balance in the plasma takes into account axial convection, the local flux of oxygen between phases, and radial diffusion in the plasma. Equations that relate the interphase flux to the local RBC and plasma oxygen tensions are based on solutions of equations analogous to Eqs. 17 and 18 for the intracellular region and on a solution for the boundary layer resistance in the plasma immediately adjacent to the RBC.

Detailed calculations of oxygen release and uptake in a 27-μm-diameter microvessel yielded results that were found to be in excellent agreement with measurements performed in the artificial capillary system of Boland *et al.* (8–10). Excellent agreement also was found with the measurements of oxygen transport in 100-μm-diameter conduits by Schmukler and Chien (76).

The calculated oxygen tension distributions by Nair *et al.* (62–64) revealed that, in the 27-μm microvessel, only approximately 4% of the resistance to oxygen transport was associated with processes within and in the near vicinity of the RBCs. This finding suggested that the model could be dramatically simplified without compromising accuracy by invoking two simplifying assumptions: 1) within the RBCs we have chemical equilibrium between oxygen and oxyhemoglobin and negligible concentration gradients; and 2) locally, the plasma and hemoglobin in the RBCs are in equilibrium. The second assumption means that the oxygen tension is continuous across the RBC membrane, but, of course, this depends on both radial and axial positions. Under these assumptions the model was simplified to a single partial differential equation, Eq. 23.

$$\left[(1 - h)v_{pl} + \left(\frac{\alpha_{rbc}}{\alpha_{pl}}\right) hv_{rbc}\left(1 + [Hb_T]\frac{dS}{d[O_2]_{rbc}}\right)\right] \times \frac{\partial[O_2]_{pl}}{\partial z} = \frac{D_{pl}\partial}{r}\frac{\partial}{\partial r}\left[r\frac{\partial[O_2]_{pl}}{\partial r}\right] \qquad (23)$$

where $[O_2]_{rbc}$ and $[O_2]_{pl}$ represent the dissolved oxygen concentrations in the RBCs and plasma, respectively. With our assumptions, they are related at each position in space by continuity of oxygen tension, Eq. 24.

$$[O_2]_{pl} = \frac{\alpha_{pl}}{\alpha_{rbc}}[O_2]_{rbc} \qquad (24)$$

Reviewing Eq. 23 term-by-term we see that the first term on the left represents convection of dissolved oxygen in the plasma; the second term, $(\alpha_{rbc}/\alpha_{pl})hv_{rbc}$, represents

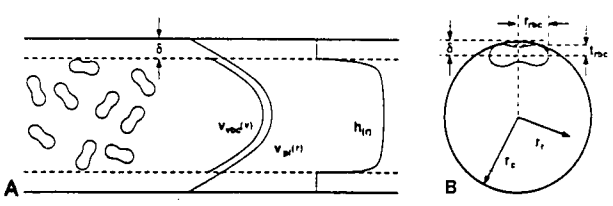

FIGURE 11. Schematic of the flow of RBCs in large capillaries. (A) RBC and plasma velocity profiles and the hematocrit profile. (B) Basis for calculation of the cell-free layer thickness, δ. (From Reference 63, with permission.)

convection of dissolved oxygen in the RBCs; and the third term, which involves the slope of the equilibrium curve, represents convection of chemically bound oxygen. Finally, the right side represents radial diffusion of oxygen.

In Eq. 23, D_{pl} is taken to be the molecular diffusivity of dissolved oxygen in the plasma. It is known of course that the RBC rotation and other motion in the shear field tends to promote radial transport. Therefore, an effective D_{pl} could be used to account for this augmented transport. Estimates of this augmentation from the work of Keller (50), Diller *et al.* (16–18), and Zydney and Colton (96) suggest that the augmentation is of the same order of magnitude as is the molecular diffusivity for the highest shear rates found in arterioles. However, these estimates of augmentation are based on measurements in vessels of 300 μm in diameter and larger—an order of magnitude larger than those of main interest in this work. It is known that RBC rotation and excursions from straight streamlines are highly suppressed in small vessels (32). Therefore, the augmentation of oxygen transport is much less than is that in larger vessels. In the absence of reliable methods to determine this suppressed augmentation, the molecular diffusivity was used.

The simple model represented by Eq. 23 was found to give excellent agreement with the more comprehensive model described above.

Comparison with Experiment and with Previous Work. Extensive calculations have been made with the models. An example of results giving a comparison with previous work is given in Fig. 12. Figure 12 compares experimental data (the points) from the artificial capillary system of Boland *et al.* (8–10) to calculated results (the four curves) by using different models. Each model was used in calculations intended to simulate the conditions of the experiments.

The Krogh approach (the lowest curve), which assumes that the resistance to radial oxygen transport in the blood is negligible, gave highly erroneous results. As discussed earlier, a number of workers have treated the transport problem in the blood by treating the blood as if it were a homogeneous hemoglobin solution. Two slightly different curves for this case are shown in Fig. 12. The calculated hemoglobin solution curves of Fig. 12 have been shown (57) to agree closely with experimental results on hemoglobin solutions. The difference in the two calculated hemoglobin solution curves of Fig. 12 is a result of the fact that Reneau *et al.* (72) neglected the augmentation of oxygen transport by diffusion of oxyhemoglobin. This augmentation is taken into account in the hemoglobin solution curve. It can be seen that the treatment of blood as a hemoglobin solution gives greatly improved results over the Krogh approach, but it is still substantially in error.

Artigue and Bruley (3) developed a model that treated

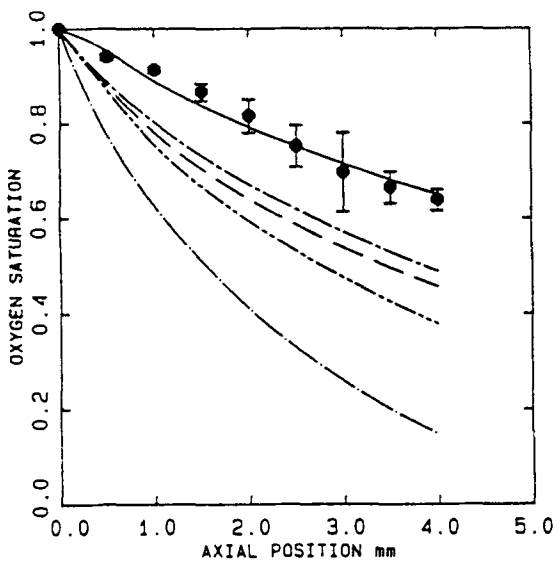

FIGURE 12. Comparison of models for oxygen release for RBC cell suspensions flowing at 12 μl/hr in a 27-μm-diameter artificial capillary. Data points, mean ± SD for experiments at 37°, with a 0.21 hematocrit suspension having a P_{50} of 20 mm/Hg used in perfusion. Curves: (—), this work; (— · —), Artigue and Bruley (3); (— —), Reneau et al. (72); (— · · —), hemoglobin solution; (— · —), Krogh-type model. (From Reference 63, with permission.)

the discrete nature of the RBCs. They lumped the resistance into two mass transfer coefficients that corresponded to the RBC-plasma interface and the plasma-capillary wall interface. The mass transfer coefficients were determined empirically. It can be seen that this model represents an improvement over the earlier work, but the results are significantly different than are those of the experimental measurements. The solid curves in Fig. 12 are simulations from the model discussed above; they give good agreement with the experimental measurements.

Uncoupling of the Intraluminal and Extraluminal Problems—the Mass Transfer Nusselt Number

In principle, the intraluminal and extraluminal transport equations are solved simultaneously and matched as solved, by conditions at the capillary wall of continuity of oxygen tension and of oxygen flux. This approach has been used by a number of workers, starting with Reneau *et al.* (72,73). However, there is a considerable incentive for uncoupling the problems (*i.e.*, for solving the intraluminal and extraluminal problems separately). Many of the most interesting and challenging current problems concern rather complex microvascular networks with heterogeneous geometrical, hemodynamic, and metabolic parameters. The complexity of these problems argues in favor of a simpler treatment of the intraluminal problem, if such treatment is possible without major sacrifice of accuracy.

Fortunately, when the intraluminal results are ex-

pressed in terms of mass transfer coefficients, the results are rather insensitive to several of the parameters so that the results of intraluminal calculations can be expressed in a concise way. For this expression, often the dimensionless mass transfer coefficient, the Nusselt number,[4] defined by Eq. 25 is used:

$$Nu = \frac{j_w d_c}{D_{pl}\alpha_{pl}(P^* - P_w)} \tag{25}$$

where d_c is the capillary diameter.

All quantities in the equation must be averaged over an axial length encompassing both an RBC and a plasma gap. However, all of the quantities are local in the sense that they are evaluated at one particular axial position along the capillary, rather than being averaged over the length of the capillary. The Nusselt number of Eq. 25 is designated as a local Nusselt number. Fortunately, for the low Reynolds and Peclet numbers that are of most interest in the microcirculation, the Nusselt number changes only slowly with oxygen saturation, as shown by Federspiel and Popel (27) and by Wang and Popel (91), so that the difference between local and average Nusselt numbers is small.

In using Nusselt numbers from various sources it is important to note that other definitions have been used. In place of d_c, in Eq. 25, some workers use r_c, capillary radius (*e.g.*, Eq. 20). In that case, the Nusselt number would be one half as large for the same oxygen flux. Similarly, some workers use D_{rbc}, the oxygen diffusivity in the intracellular hemoglobin solution, instead of D_{pl}. That change would yield a Nusselt number approximately 2.8 times larger for the same oxygen flux. In some work, the mixed mean P_{O_2} is used instead of P^*. This change has been shown by Wang and Popel (91) to make only very small differences in the Nusselt number. P^* is a useful choice, because the mixed mean oxygen saturation, S_{mm}, is the saturation that can be obtained from a material balance. A mixed mean value of a quantity is simply defined to be the value one would obtain if the blood at a given axial position were discharged into a reservoir and mixed.

The utility of S_{mm} is illustrated by the simple material balance

$$Q_{rbc}\frac{\partial}{\partial z}\{[O_2]_{mm} + S_{mm}[Hb_T]\} = 2\pi r_c j_w \tag{26}$$

where Q_{rbc} is the axial volumetric flow rate of RBCs, in, for example, cm^3/s and the quantity in { } represents the total of the dissolved and chemically bound oxygen concentrations. Formally, the mixed mean saturation is defined by Eq. 27, for the special case of the cylindrical slug of hemoglobin:

$$S_{mm} = \frac{1}{\pi a^2}\int_0^a 2\pi r S dr \tag{27}$$

where a is the radius of the cylindrical RBC, and S is the oxygen saturation which varies with radial and axial position.

For larger conduits in which there is a hematocrit distribution given by the function, h(r), we have the definition:

$$S_{mm} = \frac{1}{\pi r_c^2 H_D \langle v_{rbc}\rangle}\int_0^{r_c} 2\pi r h S v_{rbc} dr \tag{28}$$

where H_D is the overall hematocrit, a mixed mean or discharge hematocrit (see the discussion after Eq. 31) and $\langle v_{rbc}\rangle$ is the mean RBC velocity defined by

$$\langle v_{rbc}\rangle = \frac{Q_{rbc}}{\pi r_c^2} \tag{29}$$

The mixed mean concentration of a solute distributed in both the plasma and RBCs is given (using oxygen for example) by

$$[O_2]_{mm} = \frac{1}{Q}\left\{\int_0^{r_c} 2\pi r h v_{rbc}[O_2]_{rbc} dr + \int_0^{r_c} 2\pi r(1 - h)v_{pl}[O_2]_{pl} dr\right\} \tag{30}$$

where the RBCs and plasma are treated separately because they may have different solute concentrations and different velocities.

Numerical Values of the Mass Transfer Coefficients for Oxygen Delivery to the Wall of Microvessels

In this section mass transfer coefficients are presented based on the work that is judged to give the most accurate prediction of oxygen fluxes at the present time. There are two regimes in which literature seems to be on a solid basis:

1) The model outlined previously which is intended for use in microvessels in the arteriolar size range (20 μm in diameter and larger); and 2) Several workers have made calculations for capillary-sized vessels using the model in which the solid cylindrical geometrical simplification was invoked. Of the several studies that yielded similar results, the findings of Groebe and Thews (38) were selected for presentation here, because they used the most complete model, which included the influence of RBC motion. Groebe and Thews (38) reported mass transfer coefficients for a configuration consisting of the lumen of the capillary plus the endothelium and interstitial space adjacent to the exterior of the capillary. The data points to be presented in

[4]What we call the Nusselt number for mass transfer here is called the Sherwood number by some workers. These workers prefer to reserve the Nusselt number for its original use in the analogous heat transfer problem.

this section were calculated from the reported results by subtraction of the extraluminal resistance. This calculation puts all points on the same basis: all represent the luminal resistance to oxygen transport only.

For practical purposes the results are expressed in terms of the Nusselt number, *Nu*, as defined by Eq. 25. Results are shown in Fig. 13 for a hematocrit of 25%. As shown previously (27), the Nusselt numbers for the capillary-sized vessels are almost independent of hemoglobin oxygen saturation, and the lowest curve of Fig. 13 assumes that is the case. Even for the arteriolar-sized vessels the Nusselt number changes rather slowly with oxygen saturation (*e.g.*, a decrease in oxygen saturation from 80 to 40% decreases the Nusselt number only by approximately 10%). Therefore, the use of average Nusselt numbers throughout a vessel of a given diameter gives an accurate approximation of the oxygen delivery. In addition, in flow there is a distinction between space-averaged oxygen saturation (the saturation measured with a spectrophotometer; the *abscissa* of Fig. 13), and the mixed-mean saturation. The difference is not large in practical problems, and the Nusselt number is sufficiently insensitive to changes in oxygen saturation to permit us to ignore the distinction for the purpose of prediction of Nusselt numbers.

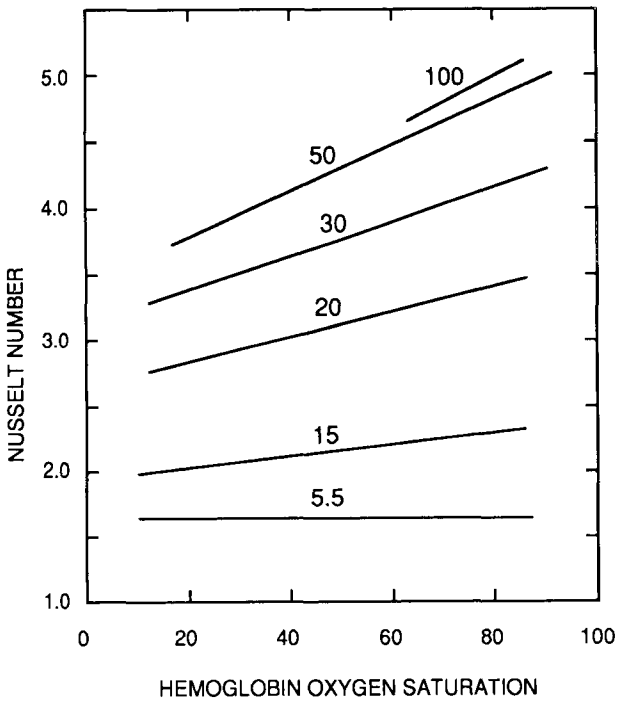

FIGURE 13. Nusselt numbers for oxygen release in microvessels of a range of diameters calculated by the solid cylinder rbc model (the 5.5-μm-diameter curve) or by the large microvessel model (all other curves). In all cases the tube hematocrit is 25%. Parameters on the curves are microvessel diameter in μm. (The large microvessel results are modified from References 62 and 63. The results for the 5.5 μm diameters calculated from the work of Groebe and Thews (37) are as explained in the text.)

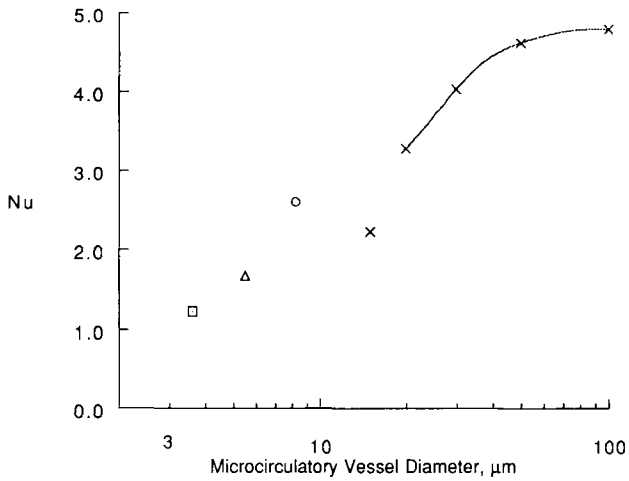

FIGURE 14. Nusselt numbers for oxygen release derived from the calculations of several workers for a range of microvessel diameters. All values are for a tube hematocrit of approximately 25% and for a hemoglobin oxygen saturation of 70%. No curve is drawn in the lower, central range of microvessel diameters because this is the region of greatest uncertainty. The points derived from various work are: Nair (62) and Nair, *et al.* (63), (x); Wang and Popel (91), (o); Groebe and Thews (37), (Δ); and Secomb and Hsu (78), ( ).

Figure 14 gives results in a form that emphasizes the importance of the vessel diameter in estimation of Nusselt numbers. The upper part of the curve, microvessel diameters of 20 μm and larger, is on a solid basis, having been calculated by a model validated by *in vitro* experiments, the large microvessel model discussed above. The point for a 5.5-μm-diameter capillary was derived from the work of Groebe and Thews (38) as discussed above. The lowest point, for a diameter of 3.6 μm, also was calculated by use of a solid cylinder model by Secomb and Hsu (77). In the central region of Fig. 14, no curve is shown. The curve was omitted to emphasize that this is range of diameters of the most uncertainty. There are no satisfactory models in this size range of microvessels. The one point in this region, for an 8.24-mm diameter vessel, is from the work of Wang and Popel (91). The point for a 15-μm-diameter vessel is almost certainly outside the range of validity of the assumptions of the large microvessel model. Therefore, it was not connected by the curve. Between the 5.5-μm point and the 20-μm point there is no way presently to estimate oxygen fluxes other than by interpolation between the two points. The capability of mathematical (or experimental) simulation does not extend to this range of diameters.

The Nusselt numbers for the larger microvessels are only weakly dependent on hematocrit. Nair (62) made calculations for a wide range of hematocrits and found an approximately linear increase of *Nu* with hematocrit over a range from 17 to 42%. Based on these results, a good estimate of the Nusselt number for a hematocrit in this range can be obtained from Eq. 31

$$Nu = Nu_{25} + (H - 25)(8.4 \times 10^{-3}) \quad (31)$$

where Nu_{25} is the Nusselt number for a hematocrit of 25%. For example, by Eq. 31, the *Nu* for a 35% hematocrit would be higher than that for a 25% hematocrit by 0.08 dimensionless units, assuming conditions other than hematocrit were the same. It should be emphasized that Eq. 31 applies to vessels of 20 μm in diameter and larger. The dependence on hematocrit is very different for capillaries, as discussed below. The term hematocrit and the unembellished symbol H are used herein to denote the "tube" hematocrit—the hematocrit that would be measured if all of the cells in the tube could be enumerated instantaneously. The "discharge" hematocrit, H_D, is the hematocrit that would be measured if the flow were to be discharged into a large container and mixed. It is the same as the mixed-mean hematocrit. The discharge hematocrits are higher than are tube hematocrits because the RBCs move at a higher than average blood velocity. Gaehtgens *et al.* (31) have presented correlations for relating tube hematocrits to discharge hematocrits as a function of the microvessel diameter and flow rate. For example, the 25% hematocrit in a 30-μm vessel of Figs. 13 and 14 is equivalent to a discharge hematocrit of 30%.

In contrast to the larger vessels, for small capillaries, *Nu* depends markedly on hematocrit, as clearly demonstrated by Federspiel and Sarelius (28) and Federspiel and Popel (27) and as discussed above. These workers also pointed out that the *Nu*-cell spacing relationship should approximate a hyperbolic form at large cell spacing. The average mass flux per RBC diminishes approximately with the reciprocal of the spacing at large spacing.

Figure 15 gives the calculated dependence of *Nu* on L_R/L_P where L_R is the "length" of the RBC (8 μm for human cells; 5.25 μm for canine cells). L_P is the edge-to-edge cell spacing. Use of this inverse variable causes the curve to pass through the origin and tends to linearize the relationship near the origin. Because the length and volume of the solid cylinder model cell agree approximately with that of an actual RBC, it is reasonable to interpret the spacing variable in terms of hematocrit. The calculated hematocrits are given along the top of the Fig. 15. The extreme importance of hematocrit as a determinant of *Nu* is illustrated by the observation that increasing the hematocrit from 20 to 30% would increase the *Nu* by approximately 50%.

The *Nu* is used in practical calculations to relate the intraluminal oxygen tension to the capillary wall oxygen tension and capillary wall oxygen flux. Rearrangement of Eq. 25 gives an expression for the intraluminal oxygen tension difference

$$P^* - P_w = \frac{j_w d_c}{D_{pl}\alpha_{pl} Nu} \quad (32)$$

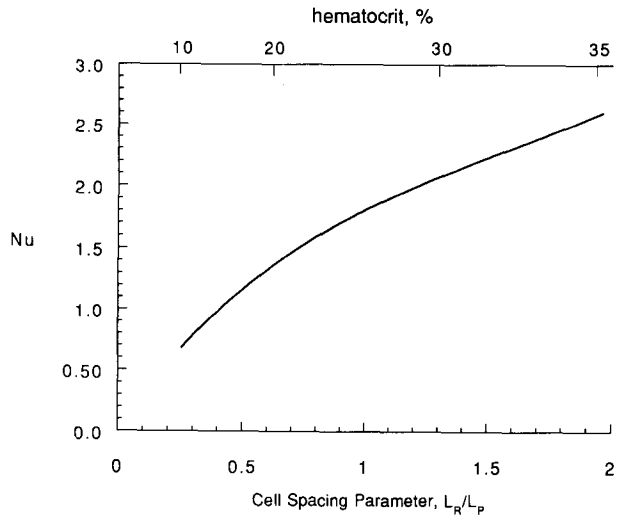

FIGURE 15. Nusselt numbers calculated for a 5.5-μm-diameter capillary at various hematocrits or RBC spacings. Results are based on RBCs idealized as solid cylinders of 4 μm in diameter. L_R denotes the RBC length, and L_P denotes the edge-to-edge axial length of the plasma gaps between the RBCs. Derived from the work of Groebe and Thews (37) as explained in the text.

Substitution of the numerical values given below yields a working formula, Eq. 33

$$D_{pl} = 2.18 \times 10^5 \text{ cm}^2\text{sec}$$
$$\alpha_{pl} = 1.34 \times 10^{-9} \text{ g moles/(cm}^3 \cdot \text{torr)}$$

$$P^* - P_w = 3.42 \times 10^9 \frac{j_w d_c}{Nu} \quad (33)$$

where d_c is in μm, j_w is in g moles/(sec · cm^2), and both P* and P_w are in torr.

Comparisons of Calculated Results with In Vivo *Results*

Experimental Oxygen Fluxes. A number of comparisons have been made of calculated and measured distributions of oxygen tension and myoglobin saturation in tissue, including capillary networks of various configurations and degrees of complexity. The great majority of these studies used a Kroghian treatment, which neglects intraluminal resistance to oxygen transport. Notable exceptions are the work of Groebe and Thews (38), discussed above and the recent work of Secomb and Hsu (77). Secomb and Hsu (77) treated a tissue region containing both arterioles and capillaries, taking the intraluminal resistance to oxygen transfer into account in all the vessels by use of mass transfer coefficients in the way discussed in the previous sections. They treated the diffusion problem by a Green's function method and obtained results for the capillary oxygen saturations that were shown to be in reasonably good agreement with the measurements of Pittman and Ellsworth (68).

It should be emphasized that these overall comparisons of oxygen concentrations distributions in a complex system do not constitute a critical test of the accuracy of any subset of the calculation procedures. A critical test of an intraluminal transport model would require detailed measurements on a smaller space scale. Ideally, we would have experimental determinations of capillary wall oxygen fluxes and oxygen tensions in addition to capillary mean oxygen saturations or tensions. Such detailed measurements have been made *in vitro* on microvessels in the arteriolar size range. However, there are no *in vitro* data on microvessels smaller than 27 μm in diameter. *In vivo*, there are substantial difficulties in obtaining the accurate, detailed data needed for a critical test of a mathematical model. Therefore, *in vivo* data that can serve to critically test models of intraluminal transport processes do not seem to exist. All that we do at present is determine whether there are any obvious inconsistencies between the intraluminal models and the *in vivo* data.

Tateishi *et al.* (84) have reported oxygen flux data for individual microvessels in a rat mesentery as shown in Fig. 16. For an arteriolar vessel with a diameter of 20 μm, the measured oxygen flux was approximately 6×10^{-6} g M/(sec · m^2), or 6×10^{-10} g M/(sec · cm^2). From Fig. 12 we estimate the Nusselt number to be 3.2. Application of Eq. 33 gives a calculated luminal oxygen tension gradient of 13 torr—a value not inconsistent with observations.

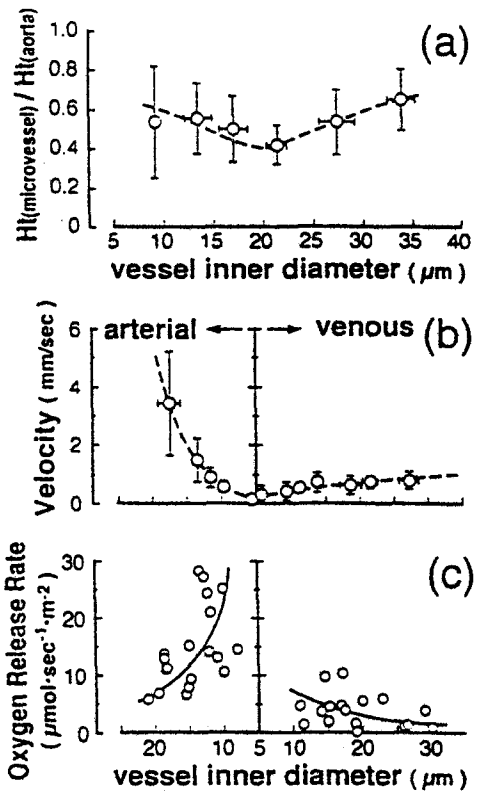

FIGURE 16. (a) Hematocrit in various microvessels relative to that in aorta (estimated spectrophotometrically). (b) Flow velocity of erythrocytes in various microvessels (arterioles, capillaries, and venules) in rat mesentery. (c) Rate of oxygen release from flowing erythrocyte measured at pH 7.4 at 30°C. (From Reference 84, with permission.)

In the 10-μm-diameter arteriole the measured flux was approximately 25×10^{-6} g mole/(sec · m^2). This diameter is in the range of uncertainty of the Nusselt numbers, as discussed earlier, but an estimate of the value would be 2.3 (based on interpolation between the points at diameters of 5.5 and 20 μm, points believed to be more reliable than other points at intermediate diameters). By using $Nu = 2.3$, Eq. 33 can be used to calculate an intraluminal oxygen tension gradient of 36 torr. The intraluminal oxygen tension (data not shown) in these experiments can be estimated from the reported oxygen saturation to be in the range of 40–45 torr. The mesentery was suffused with hydrosulfite solution to maximize the oxygen flux and oxygen tension gradient. Therefore, the calculated luminal gradient is not inconsistent with the measured fluxes.

Popel *et al.* (71) and Pittman (67) have noted a puzzling discrepancy that arose when theory and experimental measurements were compared for arteriolar oxygen fluxes in hamster muscle. The measured oxygen fluxes from both 62- and 23-μm-diameter arterioles in muscle tissue were approximately 60×10^{-6} ml O_2/(cm^2 · sec), which converts to 2.7×10^{-9} g mole/(cm^2 · sec). Popel *et al.* (71) showed that, with use of either a very simple or a more complex tissue diffusion model, this flux yielded a calculated oxygen tension drop in the tissue approximately 1 order of magnitude higher than is possible (it exceeds the measured luminal oxygen tension). Hsu and Secomb (45) used a different approach in treating the tissue diffusion problem, but they came to an equivalent conclusion: The flux computed in their model was 1 order of magnitude smaller than the experimentally observed rate of oxygen release in the capillary. Recent studies reviewed by Pittman (67) show that the discrepancy is caused in part by use of an unrealistically low tissue permeability value in the tissue diffusion calculations.

The discussion given in the previous paragraph of the puzzling large calculated oxygen tension gradient (or puzzling large measured capillary oxygen release) concerned the oxygen tension gradient in the tissue. It has not been noted previously that this measured flux also yields an unrealistically high gradient in the lumen of the arteriole. From Fig. 12 for the 23 μm capillary, we should expect the Nusselt number to be about 3.2. Using this value and the value of the flux in Eq. 23, we find:

$$P^* - P_w = \frac{(2.7 \times 10^{-9})(23)(3.42 \times 10^{9})}{3.2} = 66 \text{ torr} \tag{34}$$

This gradient is impossibly high because it is greater than

the measured luminal P_{O_2} of 32 torr. Application of the formula to the 62-μm arteriole yields a still larger luminal gradient.

Two conclusions can be drawn from these comparisons. 1) The luminal resistance to oxygen transport in arterioles is significant. It should be taken into account in any accurate simulation. However, it has been neglected by nearly all previous workers; and 2) the paradoxically high indicated gradient discussed above exists on both the luminal and abluminal sides of the microvessel wall. More accurate values of tissue permeability may lessen the abluminal paradox, but not the luminal one. Pittman (67) has discussed the experimental difficulties, and suggested that part of the discrepancy could be due to nonuniformities in the velocity and RBC distributions at the measurement sites. He pointed out that the flux calculations require the difference between values measured at two sites. Therefore, any experimental variability is amplified in the flux calculation. It is clear that more research is needed to resolve the discrepancies between theory and *in vivo* experiment.

Carbon Dioxide Transport and Acid/Base Balance

The binding of O_2 at one hemoglobin site is coupled with the binding of other substances at other sites conformational change of the hemoglobin molecule. In particular, O_2 binding to hemoglobin is affected by P_{CO_2} pH, [DPG] among other factors. In turn, O_2 binding affects binding and transport of other substances, including CO_2 and H^+. Therefore, a more complete description of gas transport required considering simultaneous interactions among hemoglobin, O_2, CO_2, H^+, and other intermediate compounds. CO_2 and O_2 exchange involve multiple interrelated physical and chemical events as depicted in Fig. 17. Because of its physiological importance, many studies have dealt with the kinetics of individual events in CO_2 exchange. However, there have been few attempts to study the integrated system by incorporating the complete set of chemical and physical events into a computational model.

The influence of carbon dioxide on oxygen transport, the Bohr effect, has been taken into account by some workers in oxygen transport simulation. Some of the approaches used have been simple and empirical. For example, Groebe (36) used measured values of the oxygen-hemoglobin equilibrium curve at arterial and venous conditions and, in the calculation procedure, used an interpolated curve that changed linearly with drop in O_2 saturation through the capillary. The few more complete treatments have used a semiempirical, lumped-parameter approach that treats blood as a homogeneous fluid and assumes local chemical equilibrium. In addition, the interdependence of all species has been represented by O_2 and CO_2 dissociation curves (3,6,11,19–21,88,89,93). Most of these previous models were developed for blood oxygenators with blood channels much greater than the dimensions of the RBC or the microvessels that are the subject of this work. There is reason to question the validity of the continuum assumption for CO_2 transport for microvessels on at least three bases. First, by analogy to the oxygen transport studies, the continuum approach tends to be inadequate when the flow channel dimension and the RBC diameter are of the same order of magnitude. Second, the local chemical equilibrium assumption is expected to be inadequate for describing extracellular CO_2 hydration/dehydration reactions, although equilibrium closely describes the chemical behavior of intracellular CO_2 in the presence of carbonic anhydrase. Third, the equilibrium approach does not incorporate the limitation to transport associated with the Cl^-/HCO_3^- RBC membrane anion exchanger.

The following section outlines a recent study (46) that has addressed the questions raised above in a model that can be considered an extension of the oxygen transport model of Nair *et al.* (64) to the much more complex case involving simultaneous O_2 and CO_2 transport.

Physical Situation

Whereas O_2 is carried by the blood mainly through a reversible chemical reaction with hemoglobin, the transport of CO_2 involves a complex interaction of many phenomena. The principal chemical and transport events that occur in blood during gas exchange in a lung capillary are shown schematically in Fig. 17. Reactions 1, 2, and 3 represent O_2 diffusion across the alveolar capillary membrane, diffusion into the RBC, and chemical reaction with intracellular hemoglobin. Under normal conditions in the human circulation, greater than 95% of the O_2 is reversibly bound to hemoglobin. The remaining O_2 is dissolved

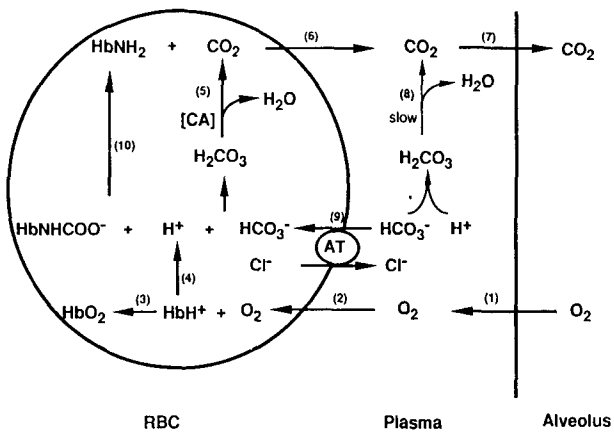

FIGURE 17. Exchange of oxygen and carbon dioxide in a pulmonary capillary (modified from References 53 and 65). (From Reference 46, with permission.)

in blood plasma and in the hemoglobin solution inside the RBCs. The remaining reactions in the respiration diagram deal with CO_2 transport and pH regulation. Under normal physiological conditions, roughly 0.7 H^+ (Bohr protons) are released from intracellular hemoglobin for each O_2, molecule that is bound (reaction 4). These acid equivalents rapidly equilibrate with HCO_3^- to produce H_2O and CO_2 because of the presence of carbonic anhydrase (represented as CA in Fig. 17). Free CO_2 then diffuses out of the cell rapidly because the plasma membrane is highly permeable to apolar gases (reaction 6). CO_2 persists in the plasma phase and then is exchanged into the alveolus (reaction 7). Therefore, reactions 5–7 allow intracellular HCO_3^- to be expelled as CO_2 in the lung. However, the bulk of venous HCO_3^-, approximately 81%, is present initially in the plasma. Because there is no extracellular carbonic anhydrase, the CO_2 dehydration reaction (reaction 8) occurs much too slowly to be of importance. Therefore, for the extracellular HCO_3^- to be evolved as CO_2 from lung capillaries, it must be transported across the RBC membrane (reaction 9). Ionized species do not cross the membrane in appreciable amounts unaided. The aid involves a one-for-one exchange of Cl^- for HCO_3^- mediated by the anion transporter (AT). Another mechanism by which CO_2 is carried by the blood is through direct reversible chemical combination with the N-terminal valines of the α- and β-chains of hemoglobin (reaction 10). In this form, 11% of the CO_2 is transported by the blood to the lung. Finally, dissolved CO_2 accounts for 8% of the CO_2 being transported to the lung. In the case of O_2 and CO_2 exchange between the blood and the respiring muscle tissues, the same processes occur in the reverse direction.

Chloride/Bicarbonate Ion Exchange Across the RBC Membrane

The experimental evidence on the exchange kinetics point toward the single-site "ping-pong" mechanism with obligatory exchange (13,26,30,49,60). The general features of the ping-pong mechanism are illustrated in Fig. 18. In the ping-pong mechanism, the anions take turns crossing the membrane rather than switching place simultaneously; and the anion exchange protein has two structurally distinct states, an inward-facing state and an outward-facing state. Therefore, it is an alternating site transporter possessing a single transport site that is alternatively exposed to the opposite sides of the membrane. This site can only cross the membrane when it is occupied by a substrate anion; it then undergoes a conformational change to face the opposite side of the membrane and releases the transported ion. The transported site can now bind another (or the same) anion and return to the original membrane

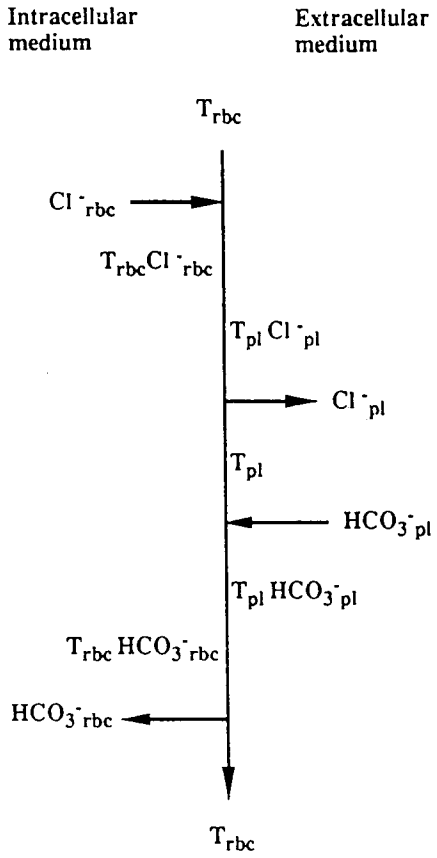

FIGURE 18. Diagram of a ping pong mechanism for anion transport. Shown here is the exchange of an intracellular Cl^- for an extracellular HCO_3^-. (From Reference 47, with permission.)

face and release the anion to complete a cycle of anion exchange. Frolich and Gunn (30) decomposed the exchange process into six steps: 1) binding of the anion to the transport molecule at one surface of the membrane, 2) translocation of the anion across the membrane, and 3) dissociation of the anion from the transport molecule at the opposite surface; followed by the opposite three steps to transport an anion back to the original surface of the membrane. Because each reaction is reversible, the mathematical description of the anion transporter involves 12 reaction velocity coefficients.

Treatment of the anion transporter at the level of detail indicated in the previous paragraph would be cumbersome. Therefore, Huang *et al.* (47), greatly simplified the kinetic expression based on the data of Falke and Chan (26). They assumed that the translocation steps are rate limiting, and, thus, the association and dissociation reactions are at equilibrium. They also assumed that the translocation rate coefficient is independent of direction and type of bound anion, and that the equilibrium association coefficients were the same on both sides of the membrane. These assumptions permit derivation of a simplified flux

expression that is mathematically more tractable and contains only two kinetic parameters, K_A, and the product $T_{tot}k_{trans}$, Eq. 35, below:

$$Flux = \frac{T_{tot}k_{trans}K_A([Cl^-]_{rbc}[HCO_3^-]_{pl} - [Cl^-]_{pl}[HCO_3^-]_{rbc})}{[CL^-]_{rbc} + [CL^-]_{pl} + [HCO_3^-]_{rbc} + [HCO_3^-]_{pl} + 2K_A\langle[CL^-]_{rbc}[Cl^-]_{pl} + [HCO_3^-]_{rbc}[HCO_3^-]_{pl} + [Cl^-]_{rbc}[HCO_3^-]_{pl} + [Cl^-]_{pl}[HCO_3^-]_{rbc}\rangle} \quad (35)$$

Where k_{trans} is the translation rate coefficient, and T_{tot} is the total number of anion transporters per RBC, K_A is the equilibrium association constant, and *Flux* denotes the HCO_3^- flux into the rbc (the negative of the Cl^- flux). Equation 35 reduces to the Donnan equilibrium expression for a net flux of zero.

The simplified ping-pong model is on a more satisfactory theoretical basis and was shown to consistently provide better agreement with the available experimental data than did the passive diffusion model used by previous workers.

The Transport Model

The anion transporter was incorporated into a model for predicting O_2 and CO_2 transport and acid/base balance in blood flowing in microvessels in an extension of the simplified model for O_2 transport described above.

In principle, differential equation mass balances are required within the RBCs for eight species (see Fig. 17), O_2, CO_2, HbO_2, $HbCO_2$, O_2HbCO_2, H^+, HCO_3^-, and Cl^-, and in the plasma for five species (all eight except the ones containing Hb). This yields a system of 13 partial differential equations. The system was reduced to seven equations by invoking the following simplifying assumptions: the RBC oxygen balance incorporates HbO_2 on the basis of assumed chemical equilibrium; the RBC CO_2 balance incorporates $HbCO_2$, O_2HbCO_2, and HCO_3^- on the basis of assumed chemical equilibrium (this balance is connected to the plasma balance through the flux expression, Eq. 35); the RBC H^+ balance incorporates the buffering capacity of the intracellular environment as well as those reactions in Fig. 17 that alter $[H^+]$, including the HCO_3^- flux; and the RBC Cl^- balance incorporates the Cl^- flux through the RBC membrane, the negative of the HCO_3^- flux. In the plasma phase we need only three equations. No O_2 or CO_2 balances are required in the plasma under the assumption than these nonpolar molecules move freely through the RBC membrane. Continuity of partial pressures across the RBC membrane is assumed. Therefore, the plasma and RBC concentrations of both O_2 and CO_2 are directly related at each point in space. H^+ and Cl^- balances in the plasma are required analogous to those in the RBC; and a HCO_3^- balance is required in the plasma. Equation 8 in Fig. 17 is too slow to be of practical importance in the absence of carbonic anhydrase. Therefore, unlike the inside of the RBC, the plasma HCO_3^- and CO_2 concentrations are not related through an equilibrium relationship.

RESULTS

The system of seven partial differential equations has been integrated for a variety of conditions and detailed results are presented elsewhere (46). A summary of some of the conclusions from the calculations is given below.

When no CO_2 transfer is incorporated in the calculations, the calculated O_2 transfer is less than in the case of simultaneous O_2 and CO_2 transfer (the Bohr effect). The Bohr effect is more significant for the deoxygenation case, than for the oxygenation case. In the example calculations it altered deoxygenation by approximately 25%, but oxygenation by only 10%. The effect of simultaneous O_2 transport on CO_2 transport, the Haldane effect, was only of secondary importance in the cases calculated. A number of commonly used drugs are known to inhibit anion exchange across the RBC membrane. Inhibition of the anion transport was shown to substantially reduce CO_2 transfer and pH changes.

Experimental results by Dorson and Voorhees (19,90) were used for comparison with the calculations from the models. These data on simultaneous O_2 and CO_2 transport seem to be the most complete of any available. The data include the relevant blood gas parameters and the biochemical status of each of the inlet and outlet blood samples. Figure 19 (A and B) shows results for O_2 uptake with CO_2 elimination in the experiments in comparison to the predictions generated by both the discrete and continuum (previous work) models. For O_2 uptake, it can be seen from Fig. 19 that the discrete model gives excellent agreement with the experiments, and that the continuum model is also fairly successful. For CO_2 elimination, Fig. 19, the discrete model is again shown to agree with the experiments, whereas the continuum model is inadequate. Figure 19 (C and D) for experiments on O_2 release with CO_2 uptake show a similar finding for the discrete model; it gives very good agreement with the experimental data. However, the continuum model is inadequate for both O_2 and CO_2 transport: it underpredicts the transport of O_2 and overpredicts the transport of CO_2. The relatively minor under prediction of the oxygen uptake of the continuum model (Fig. 19A) could be remedied by adjusting the effective diffusivity of O_2 in the model. However, this ad-

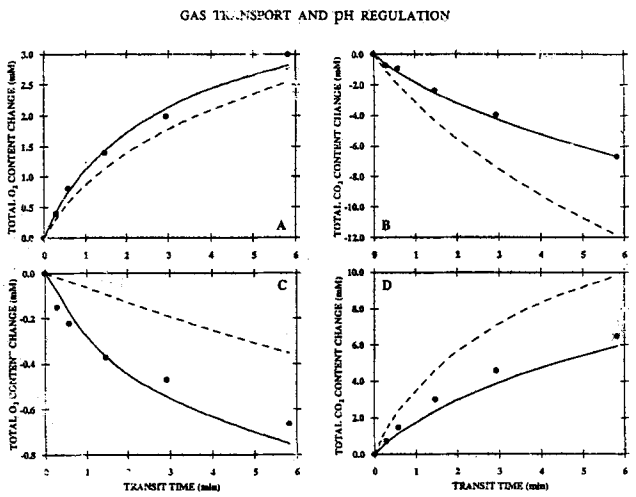

FIGURE 19. Comparison of models for oxygenation accompanied by CO_2 elimination (A and B) of RBC suspensions flowing in a 1.47-mm-diameter membrane tube at 25° with H_D = 0.43, $P_{50,in}$ = 16.8 mm Hg, $P_{O_2,in}$ = 22.7 mm Hg, $P_{CO_2,in}$ in 54.4 mm Hg, $P_{O_2,ext}$ = 708 mm Hg, and $P_{CO_2,ext}$ = 0 mm Hg. (A) Total O_2 content change as a function of transit time and (B) the total CO_2 content change. Comparison of models for deoxygenation accompanied by CO_2 uptake (C and D), $P_{50,in}$ = 17.6 mm Hg, P_{O_2in} = 22.5 mm Hg, P_{CO_2in} = 53.9 mm Hg, P_{O_2ext} = 0 mm Hg, and $P_{CO_2,ext}$ = 115 mm Hg. (C) Total O_2 content change as a function of transit time and (D) the total CO_2 content change. Data points: means of experiments from Voorhees (90). Curves: theoretical simulation curves for the same conditions; (—) the discrete model of this work, and (- - - -) the continuum model. (From Reference 47, with permission.)

justment would not have much impact on the relatively large underprediction of oxygen release (Fig. 19C).

From Fig. 19 (B and D), it is clear that, for predicting CO_2 transport, the discrete model represents an important improvement in accuracy over the continuum model. In these cases, the continuum model predicts more transport than is observed experimentally. A major factor in the success of the discrete model for predicting CO_2 transfer is the incorporation of the slow CO_2 hydration/dehydration reactions in the plasma. This conclusion was substantiated and demonstrated by considering a nonphysiological situation in which carbonic anhydrase activity equivalent to that of the RBC interior was made available to the plasma. In that case, the amount of CO_2 transfer predicted by the discrete model approached that predicted by the continuum model for both oxygenation and deoxygenation cases.

Therefore, for these relatively very large tubes, 1.47 mm in diameter, the principal advantage of the discrete model is in the incorporation of the anion exchanger and separating the bicarbonate into two compartments: intracellular (with carbonic anhydrase and, thus, a close approximation to equilibrium in reaction number 5 of Fig. 17); and extracellular (in which a zero rate of reaction 8 of Fig. 17 is approximated). For microvessels, the discrete model would be expected to be even more advantageous. Unfortunately, there are no complete data sets available for simultaneous transfer of O_2 and CO_2 in microvessels. Therefore, the model has not been tested in the circumstances in which it would be expected to be most advantageous.

DISCUSSION

Why A Half Century of Misdirection?

In reviewing the literature on mathematical simulation of oxygen delivery to tissue, one sees that virtually all mathematical simulation efforts for 50 or so years after Krogh's pioneering work were on a faulty basis, in that the important intraluminal resistance to oxygen transport was neglected. Therefore, the results of the vast majority of the early theoretical papers are, at best, of only qualitative interest. In the last two decades, the importance of the intraluminal processes in capillaries has been realized, and very significant progress has been made as outlined above. Yet, even today, with apparently only one exception (77), all simulations have continued to neglect the intraluminal resistance to oxygen transport in arterioles and venules. As we have shown, this resistance to oxygen transport is far from negligible.

So we should inquire as to how the misdirection of the many research workers could have persisted over such a long period of time. The key factor is that very detailed experimental measurements are required to critically test the simplifying assumptions that form the basis for the various simulations. Consider an example of how overall measurements are inadequate: one of the key parameters in any simulation is the tissue metabolic consumption rate of oxygen. In all simulation schemes, the parameter plays an important role in determining the oxygen flux at the capillary wall. The parameter usually is estimated from experimental measurements of changes in oxygen saturation in the blood perfusing the tissue. Then, the parameter is used to establish the boundary conditions on the differential equations used in simulation of oxygen transport. In such cases, the solution of the system of differential equations is literally bound to produce the same overall change in oxygen saturation as that which was used in the estimation of the metabolic consumption rate. Therefore, a comparison of calculated and experimental overall oxygen tension and saturation changes in the blood can be circular and not a test of the model at all.

Much more detailed distributions of local oxygen tension and hemoglobin saturation are required to critically test a model. Ideally, these measurements should include not only the oxygen saturation changes and flow rates needed to calculate the oxygen delivery from a microvessel, but also information on the boundary condition of the microvessel, such as the oxygen tension distribution on or in the near vicinity of the microvessel wall. Such mea-

surements are of the highest degree of difficulty. Therefore, such complete and detailed measurements have been made only in an *in vitro* system, and only for arteriolar-sized vessels. Thus, only one model for oxygen transport in microvessels has been critically tested. No models for transport in capillaries have been subjected to such a rigorous test.

Conversely, experimental work has made real progress in recent years, to the point where comparisons with myoglobin saturation profiles and capillary oxygen fluxes are possible. Therefore, the gross misdirection of the early years is certainly ruled out by careful workers. However, even now, there are some major unexplained discrepancies which arose in efforts to compare theory and *in vivo* experiments.

It is important to note that many previous workers who have studied oxygen transport at the organ level with a combination of mathematical and experimental methods have not neglected the intraluminal resistance to mass transfer. Typically these workers measure tissue P_{O_2} distributions [*e.g.*, the work of Schubert *et al.* (29)], and/or use indicator dilution methods after injecting labeled solutes including oxygen [*e.g.*, the work of Bassingthwaighte *et al.* (4,15)]. The results often are analyzed with the aid of mathematical simulation schemes that are one dimensional: the differential equations for luminal transport employ only the axial space dimension. Therefore, the models tacitly work with mixed-mean concentration variables. The differential equations often contain "permeability coefficients," which govern the transport between the lumen of the capillary and the extraluminal tissue. Analysis of the experimental data yields values of these permeability coefficients. Although seldom mentioned and perhaps not understood in all cases, these permeability coefficients are types of mass transfer coefficients that incorporate the intraluminal resistance, the subject of this paper, lumped with other resistances which differ in the various approaches. So the intraluminal resistance is an important component of what is reported as "capillary permeability."

Concluding Remarks

1.) Methods for prediction of oxygen transport rates appear to be well developed for relatively large microvessels—those of 20 μm diameter and larger. These methods have been validated by comparison with experiments.

2.) For capillaries, models based on the solid cylindrical RBC idealization seem to be on a sound basis, although there are no experimental data of sufficient detail and accuracy to critically test the models.

3.) For intermediate-sized microvessels (between 7 and 20 μm in diameter), there are no theoretical or experimental models for prediction of oxygen transport rates. At present, all one can do is make estimates based on interpolation between the results for models mentioned above. Obviously, there is a need for more research here.

4.) In recent years, most workers in simulation of microcirculatory transport have appreciated the importance of the intraluminal resistance to oxygen transport in capillaries. However, nearly all workers have continued to neglect the intraluminal resistance in arteriolar-size vessels. This resistance is highly significant and clearly should be taken into account.

5.) Carbon dioxide transport plays a key role in oxygen transport and acid/base balance in tissue. Treating simultaneous O_2 and CO_2 transport involves transport and reaction of several other species. However, these complexities can be treated with a highly tractable set of seven transport equations as outlined above. A key feature of the model is incorporation of the RBC membrane Cl^-/HCO_3^- anion exchanger.

6.) As we have emphasized, there remain a number of paradoxical difficulties in comparing theory and *in vivo* experiment. There is a clear need for additional research to resolve the discrepancies.

REFERENCES

1. Adair, G. S. The hemoglobin system. VI. The oxygen dissociation curve of hemoglobin. *J. Biol. Chem.* 63:529–545, 1925.
2. Aroesty, J., and J. F. Gross. Convection and diffusion in the microcirculation. *Microvasc. Res.* 2:247–267, 1970.
3. Artigue, R. S., and E. F. Bruley. The transport of oxygen, glucose, carbon dioxide and lactic acid in the human brain: Mathematical models. In: *Oxygen Transport to Tissue IV: Advances in Experimental Medicine and Biology,* edited by D. F. Bruley and H. E. Bischer. New York: Plenum Press, 1983, pp. 227–234.
4. Bassingthwaighte, J. B., and C. A. Goresky. Modeling in the analysis of solute and water exchange in the microvasculature. In: *Handbook of Physiology,* (Sect. 2, The Cardiovascular System; vol. IV, The Microcirculation, edited by E. M. Renkin and C. C. Michel. Bethesda, MD: American Physiological Society: City, 1984, pp. 549–626.
5. Baxley, P. T., and J. D. Hellums. A simple model for simulation of oxygen transport in the microcirculation. *Ann. Biomed. Eng.* 11:401–416, 1983.
6. Benn, J. A., K. A. Smith, P. A. Drinker, and B. B. Mikic. The effects of carbonic anhydrase and oxygen uptake on carbon dioxide transfer in an oxygenator. *Proc. 28th Annu. Conf. Eng. Med. Biol.* 17:241, 1975.
7. Bird, R. B., E. W. Stewart, and E. N. Lightfoot. *Transport Phenomena.* New York: John Wiley amd Sons, 1960, pp. 42–47.
8. Boland, E. J., P. K. Nair, D. D. Lemon, J. S. Olson, and J. D. Hellums. An in vitro capillary system for studies on microcirculatory O_2 transport. *J. Appl. Physiol.* 62:791–797, 1987.
9. Boland, E. J., J. S. Olson, and J. D. Hellums. Development of an in vitro method for simulation of oxygen transport in the microcirculation. In: *Oxygen Transport to Tissue VII: Advances in Experimental Medicine and Biology,* edited by F. Kreuzer, S. M. Cain, Z. Turek, and T. K. Goldstick. New York: Plenum Press, 1984, pp. 923–936.

10. Boland, E. J., H. Unno, J. S. Olson, and J. D. Hellums. An in vitro method for simulation of oxygen transport in the microcirculation. *Adv. Exp. Med. Biol.* 180:251–259, 1984.
11. Buckles, R. G., E. W. Merrill, and E. R. Gilliland. An analysis of oxygen absorption in a tubular membrane oxygenator. *Am. Inst. Chem. Eng. J.* 14:703–708, 1968.
12. Bugliarello, G., and G. C. Hsau. A mathematical model of the flow in the axial plasmatic gaps of the smaller vessels. *Biorheology* 7:5–15, 1970.
13. Cabantchik, Z. I., P. A. Knauf, and A. Rothstein. The anion transport system of the red blood cell: the role of membrane protein evaluated by the use of probes, *Biochim. Biophys. Acta* 515:239–302, 1978.
14. Clark, A., W. J. Federspiel, P. A. A. Clark, and G. R. Cokelet. Oxygen delivery from red cells. *Biophys. J.* 47: 171–181, 1985.
15. Deussen, A., and J. B. Bassingthwaighte. Modeling ^{15}O-oxygen tracer data for estimating oxygen consumption. *Am. J. Physiol.* 1995, in press.
16. Diller, T. E., and B. B. Mikic. Oxygen diffusion in blood: a translational model of shear-induced augmentation. *J. Biomech. Eng.* 105:346–352, 1983.
17. Diller, T. E., B. B. Mikic, and P. A. Drinker. Shear-induced augmentation of oxygen transfer in blood. *J. Biomech. Eng.* 102:67–72, 1980.
18. Diller, T. E., I. A. Pattantyus, and W. C. Gritts. Augmentation and facilitation of oxygen transfer in flowing hemoglobin solutions. *Adv. Exp. Med. Biol.* 180:545–550, 1984.
19. Dorson, W. J. Mass transfer modeling for membrane oxygenation. In: *Artificial Organs*, edited by W. J. Kolff. London: Macmillian & Co., 1977, pp. 39–49.
20. Dorson, W. J., K. G. Larsen, R. J. Elgas, and M. E. Voorhees. Oxygen transfer to blood: Data and theory. *Trans. Am. Soc. Artif. Int. Organs* XVII:309–316, 1971.
21. Dorson, W. J. and M. Voorhees. Limiting models for the transfer of CO_2 and O_2 in membrane oxygenators. *Trans. Am. Soc. Artif. Int. Organs* XX:219–226, 1974.
22. Duda, J. L., and J. S. Vrentas. Steady flow in the region of closed streamlines in a cylindrical cavity. *J. Fluid Mech.* 45:247–261, 1971.
23. Duling, B. R., and R. M. Berne. Longitudinal gradients in periarteriolar oxygen tension. *Circ. Res.* 27:669–676, 1975.
24. Duling, B. R., and R. N. Pittman. Oxygen tension: dependent or independent variable in local control of blood flow. *Fed. Proc.* 34:2012–2019, 1975.
25. Fair, J. C., and M. H. Weissman. Oxygen transfer to blood flowing in round tubes including Bohr and Haldane effects. *Chem. Eng. Sci.* 26:963–967, 1971.
26. Falke, J. J., and S. I. Chan. Evidence that anion transport by band 3 proceeds via a ping-pong mechanism involving a single transport site. *J. Biol. Chem.* 260:9537–9544, 1985.
27. Federspiel, W. J., and A. S. Popel. A theoretical analysis of the effect of the particulate nature of blood on oxygen release in capillaries. *Microvasc. Res.* 32:164–189, 1986.
28. Federspiel, W. J., and I. H. Sarelius. An examination of the contribution of red cells spacing to the uniformity of oxygen flux at the capillary wall. *Microvasc. Res.* 27:273–285, 1984.
29. Fletcher, J. E., and R. W. Schubert. Axial diffusion and wall permeability effects in perfused capillary-tissue structure. *BioSystems* 20:153–174, 1987.
30. Frohlich, O., and R. B. Gunn. Erythrocyte anion transport: the kinetics of a single-site obligatory exchange systems. *Biochim. Biophys. Acta* 864:169–194, 1986.
31. Gaehtgens, P., K. H. Albrecht, and F. Kreutz. Fahraeus effect and cell screening during tube flow of human blood. I. Effect of variation of flow rate. *Biorheology* 15:147–154, 1978.
32. Gaehtgens, P., C. Duhrssen, and K. H. Albrecht. Motion, deformation, and interaction of blood cells and plasma during flow through narrow capillary tubes. *Blood Cells* 6:799–812, 1980.
33. Gayeski, T. E. J., and C. R. Honig. O_2 gradients from sarcolemma to cell interior in red muscle at maximal V_{O_2}. *Am. J. Physiol.* 251:H789–H799, 1986.
34. Gayeski, T. E. J., and C. R. Honig. Intracellular P_{O_2} in long axis of individual fibers in working dog gracilis muscle. *Am. J. Physiol.* 254:H1179–H1186, 1988.
35. Groebe, K. A versatile model of steady state O_2 supply to tissue: application to skeletal muscle. *Biophys. J.* 57:485–498, 1990.
36. Groebe, K. An easy-to-use model for O_2 supply to red muscle: validity of assumptions, sensitivity to errors in data. *Biophys. J.* 68:1246–1269, 1995.
37. Groebe, K., and Thews, G. Theoretical analysis of oxygen supply to contracted skeletal muscle. *Adv. Exp. Med. Biol.* 200:495–514, 1986.
38. Groebe, K., and G. Thews. Effects of cell spacing and red cell movement upon oxygen release under conditions of maximally working skeletal muscle. *Adv. Exp. Med. Biol.* 248:175–184, 1989.
39. Hellums, J. D. The resistance to oxygen transport in the capillaries relative to that in the surrounding tissue. *Microvasc. Res.* 13:131–136, 1977.
40. Hellums, J. D. Deformation of blood cells in capillaries: a commentary. *Blood Cells* 6:815–817, 1980.
41. Hill, A. V. The possible effects of the aggregation of the molecules of haemoglobin on its dissociation curve. *J. Physiol. (Lond.)* 41:iv, 1910.
42. Hochmuth, R. M., R. N. Marple, and S. P. Sutera. Capillary blood flow. I. Erythrocyte deformation in glass capillaries. *Microvasc. Res.* 2:409–417, 1970.
43. Homer, L. D., P. K. Weathersby, and L. A. Kiesow. Oxygen gradients between red blood cells in the microcirculation. *Microvasc. Res.* 22:308–323, 1981.
44. Honig, E. R., T. E. J. Gayeski, W. Federspiel, A. Clark, and P. Clark. Muscle oxygen gradients from hemoglobin to cytochrome: new concepts, new complexities. *Adv. Exp. Med. Biol.* 169:23–28, 1984.
45. Hsu, R., and T. W. Secomb. Analysis of oxygen exchange between arterioles and surrounding capillary-perfused tissue. *J. Biomech. Eng.* 114:227–231, 1992.
46. Huang, N. S., and J. D. Hellums. A theoretical model for gas transport and acid/base regulation by blood flowing in microvessels. *Microvasc. Res.* 48:364–388, 1994.
47. Huang, N. S., J. D. Hellums, and J. S. Olson. Mathematical simulation of gas transport and acid/base regulation by blood flowing in microvessels: the Cl^-/HCO_3^- exchange across the red cell membrane. In: *Oxygen Transport to Tissue XV: Advances in Experimental Medicine and Biology*, edited by P. Vaupel. New York: Plenum Press, 1994, pp. 167–174.
48. Hyman, W. A. A simplified model of the oxygen supply function of capillary blood flow. In: *Advances in Experimental Medicine and Biology*, edited by D. F. Bruley and H. E. Bicher. New York: Plenum Press, 1973, pp. 835–871.
49. Jennings, M. L. Structure and function of the red blood cell

anion transport protein, *Ann. Rev. Biophys. Chem.* 18:397–430, 1989.
50. Keller, K. H. Effect of fluid shear on mass transport in flowing blood. *Fed. Proc.* 30:5, 1971.
51. Keller, K. H., and E. K. Friedlander. The steady-state transport of oxygen through hemoglobin solutions. *J. Gen. Physiol.* 49:663–679, 1966.
52. Klocke, R. A. Carbon dioxide transport. In: *Handbook of Physiology,* edited by L. E. Farhi and S. M. Ternney. Bethesda, MD: American Physiology Society, 1987, pp. 173–198.
53. Knisley, M. H., D. D. Reneau, and D. F. Bruley. The development and use of equations for predicting the limits on the rates of oxygen supply to the cells of living tissue and organs. *Angiology* 20:1–56, 1969.
54. Krogh, A. The number and distribution of capillaries in muscles with calculations of the oxygen pressure head. *J. Physiol.* 52:409–415, 1919.
55. Krogh, A. *The Anatomy and Physiology of Capillaries.* New Haven, CT: Yale University Press, 1922, 000 pp.
56. Kutchai, H., and N. C. Staub. Steady-state, hemoglobin-facilitated O_2 transport in human erythrocytes. *J. Gen. Physiol.* 53:576–589, 1969.
57. Lemon, D. D., P. K. Nair, E. J. Boland, J. S. Olson, and J. D. Hellums. Physiological factors affecting O_2 transport by hemoglobin in an in vitro capillary system. *J. Appl. Physiol.* 62:798–806, 1987.
58. Lightfoot, E. N., Jr. In: *Transport Phenomena in the Cardiovascular System.* New York: Wiley, 1972, pp. 334–343.
59. Lih, M. M. A mathematical model for the axial migration of suspended particles in tube flow. *Bull. Math. Biophys.* 31: 143–152, 1969.
60. Lowe, A. G., and A. Lamber. Chloride-bicarbonate exchange and related transport processes. *Biochim. Biophys. Acta* 694:353–374, 1983.
61. Moll, W. The influence of hemoglobin diffusion on oxygen uptake and release by red cells. *Respir. Physiol.* 6:1–15, 1969.
62. Nair, P. K. Simulation of Oxygen Transport in Capillaries. Houston: Rice University, Ph.D. Thesis, 1988.
63. Nair, P. K., J. D. Hellums, and J. S. Olson. Prediction of oxygen transport rates in blood flowing in large capillaries. *Microvasc. Res.* 38:269–285, 1989.
64. Nair, P. K., N. S. Huang, J. D. Hellums, and J. S. Olson. A simple model for prediction of oxygen transport rates by flowing blood in large capillaries. *Microvasc. Res.* 39:203–211, 1990.
65. Nunn, J. F. *Applied Respiratory Physiology.* New York: Butterworths, 1987, 000 pp.
66. O'Riordan, J. F., T. K. Goldstick, J. Ditzel and J. T. Ernest. Characterization of oxygen-hemoglobin equilibrium curves using nonlinear regression of the Hill equation: parameter values for normal adults. *Adv. Exp. Med. Biol.* 159:435–444, 1983.
67. Pittman, R. N. Influence of microvascular architecture on oxygen exchange in skeletal muscle. *Microcirculation* 2:1–18, 1995.
68. Pittman, R. N., and M. L. Ellsworth. Estimation of red cell flow in microvessels: Consequences of the Baker-Wayland spatial averaging model. *Microvasc. Res.* 32:371–388, 1986.
69. Popel, A. S. Theory of oxygen transport to tissue. *Crit. Rev. Biomed. Eng.* 17:257–321, 1989.
70. Popel, A. S., and J. F. Gross. Analysis of oxygen diffusion from arteriolar networks. *Am. J. Physiol.* 237(6):H681–H689, 1979.
71. Popel, A. S., R. N. Pittman, and M. L. Ellsworth. Rate of oxygen release from arterioles is an order of magnitude higher than expected. *Am. J. Physiol.* 256:H921–H924, 1989.
72. Reneau, D. D., D. F. Bruley, and M. H. Knisley. A mathematical simulation of oxygen release, diffusion and consumption in the capillaries and tissue of the human brain. In: *Chemical Engineering in Medicine and Biology,* edited by D. Hershey. New York: Plenum Press, 1967, pp. 135–241.
73. Reneau, D. D., D. F. Bruley, and M. H. Knisley. A digital simulation of transient oxygen transport in capillary tissue systems (cerebral grey matter). *Am. Inst. Chem. Eng. J.* 15:916–925, 1969.
74. Salathe, E. P. Mathematical modeling of oxygen transport in skeletal muscle. *Math. Biosci.* 58:171–177, 1982.
75. Salathe, E. P., T. C. Wang, and J. C. Gross. Mathematical analysis of oxygen transport to tissue. *Math. Biosci.* 51:89–96, 1980.
76. Schmukler, R., and S. Chien. Rapid deoxygenation of red cells and hemoglobin solution using hollow capillary fibers. *Biorheology* 22:21–29, 1985.
77. Secomb, T. W., and R. Hsu. Simulation of O_2 transport in skeletal muscle: diffusive exchange between arterioles and capillaries. *Am. J. Physiol.* 267:H1214–H121, 1994.
78. Secomb, T. W., M. Intaglietta, and J. F. Gross. Effects of vasomotion on microcirculatory mass transport. In: *Vasomotion and Flow Modulation in the Microcirculation,* Prog. Appl. Microcirc. edited by M. Intaglietta. Basel, Switzerland: Karger, 1989, pp. 49–61.
79. Seshadri, V., R. M. Hochmuth, P. A. Groce, and S. P. Sutera. Capillary blood flow. II. Deformable model cells compared to erythrocytes *in vitro. Microvasc. Res.* 2:434–442, 1970.
80. Sheth, B. V., and J. D. Hellums. Transient oxygen transport in hemoglobin layers under conditions of the microcirculation. *Ann. Biomed. Eng.* 8:183–196, 1980.
81. Sinha, R. Untersuchungen uber die Viskositat von Suspensionen und Losungen. *Kolloid. Z.* 76:16–24, 1936.
82. Skalak, R., and P.-I. Branemark. Deformation of red blood cells in capillaries. *Science* 164:717–722, 1969.
83. Stewart, R. R., and C. A. Morrazzi. Oxygen transport in the human brain—Analytical solution. In: *Advances in Experimental Medicine and Biology,* edited by D. F. Bruley and H. E. Bicher. New York: Plenum Press, 1973, pp. 843–848.
84. Teteishi N., N. Maeda, and T. Shiga. A method for measuring the rate of oxygen release from single microvessels. *Circ. Res.* 70:812–819, 1992.
85. Thews, G. Oxygen diffusion in the brain: a contribution to the question of the oxygen supply of the organs. *Arch. Ges. Physiol.* 271:197–205, 1960.
86. Vandegriff, K. D., and J. S. Olson. Morphological and physiological factors affecting oxygen uptake and release by red blood cells. *J. Biol. Chem.* 259:12619–12627, 1984a.
87. Vandegriff, K. D., and J. S. Olson. The kinetics of O release by human red blood cells in the presence of external sodium dithionite. *J. Biol. Chem.* 259:12609–12618, 1984b.
88. Villarroel, F., C. E. Lanham, K. B. Bischoff, T. M. Regan, and J. M. Calkins. Gas transport to blood flowing in semipermeable tubes under steady and pulsatile flow conditions. *Chem. Eng. Progr. Symp. Ser.* 67:96–104, 1971.

89. Villarroel, F., and E. E. Lanham. A design calculation method for capillary-tube oxygenators. *Med. Biol. Eng.* 11: 732–742, 1973.
90. Voorhees, M. E. Mutual Transfer of Carbon Dioxide and Oxygen to and from Blood Flowing in Macrochannel Devices. Arizona State University, Tempe, AZ, Ph.D. Thesis, 1976.
91. Wang, C. H., and A. S. Popel. Effect of red blood cell shape on oxygen transport in capillaries. *Math. Biosci.* 116: 89–110, 1993.
92. Weerappuli, D. P. V., and A. S. Popel. A model of oxygen exchange between an arteriole or venule and the surrounding tissue. *J. Biomech. Eng.* 111:24–31, 1989.
93. Weissman, M. H., and L. F. Mockros. Oxygen and carbon dioxide transfer in membrane oxygenators. *Med. Biol. Eng.* 7:169–184, 1969.
94. Yap, E. W., and J. D. Hellums. Use of Adair four-step kinetics in mathematical simulation of oxygen transport in the microcirculation. *Adv. Exp. Med. Biol.,* 215:193–207, 1987.
95. Zarda, P. R., S. Chien, and R. Skalak. Interaction of viscous incompressible fluid with an elastic body. Symp. Fluid-Structure Interaction, ASME, New York, 1977, pp. 65–82.
96. Zydney, A. L., and C. K. Colton. Augmented solute transport in the shear flow of a concentrated suspension. *PhysicoChem. Hydrodynamics,* 10:77–96, 1988.
97. Groebe, K., and G. Thews. Calculated intra- and extracellular P_{O_2} gradients in heavily working red muscle. *Am. J. Physiol.* 259 (*Heart Circ. Physiol.* 28):H84–H92, 1990.